CR-91-0034-1

AD

Reports Control Symbol
OSD - 1366

ANALYSIS AND MITIGATION OF OPTICAL TURBULENCE EFFECTS

June 1991

Charles L. Rino
Angela Regalia

Vista Research, Inc
100 View Street
Mountain View, CA 94042

Under Contract DAAL07-86-C-0034
Contract Monitor Jennifer C. Ricklin

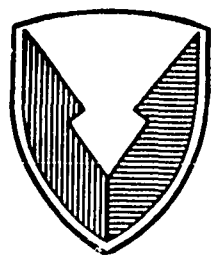

Approved for public release; distribution unlimited.

US ARMY
LABORATORY COMMAND

ATMOSPHERIC SCIENCES LABORATORY
White Sands Missile Range, NM 88002-5501

NOTICES

Disclaimers

The findings in this report are not to be construed as an official Department of the Army position, unless so designated by other authorized documents.

The citation of trade names and names of manufacturers in this report is not to be construed as official Government indorsement or approval of commercial products or services referenced herein.

Destruction Notice

When this document is no longer needed, destroy it by any method that will prevent disclosure of its contents or reconstruction of the document.

SECURITY CLASSIFICATION OF THIS PAGE

REPORT DOCUMENTATION PAGE

1a. REPORT SECURITY CLASSIFICATION UNCLASSIFIED	1b. RESTRICTIVE MARKINGS
2a SECURITY CLASSIFICATION AUTHORITY	3. DISTRIBUTION/AVAILABILITY OF REPORT Approved for public release; distribution unlimited
2b. DECLASSIFICATION/DOWNGRADING SCHEDULE	
4. PERFORMING ORGANIZATION REPORT NUMBER(S) Delivery Order	5. MONITORING ORGANIZATION REPORT NUMBER(S) ASL-CR-91-0034-1
6a NAME OF PERFORMING ORGANIZATION Vista Research, Inc. — 6b. OFFICE SYMBOL (If applicable)	7a. NAME OF MONITORING ORGANIZATION U.S. Army Research Office
6c. ADDRESS (City, State, and ZIP Code) 100 View St., P.O. Box 998 Mountain View, CA 94042	7b. ADDRESS (City, State, and ZIP Code) P.O. Box 12211 Research Triangle Park, NC 27709-2211
8a. NAME OF FUNDING/SPONSORING ORGANIZATION U.S. Army Atmospheric Sciences Laboratory — 8b OFFICE SYMBOL (If applicable)	9. PROCUREMENT INSTRUMENT IDENTIFICATION NUMBER
8c ADDRESS (City, State, and ZIP Code) White Sands Missile Range, NM 88002-5501	10 SOURCE OF FUNDING NUMBERS PROGRAM ELEMENT NO | PROJECT NO | TASK NO | WORK UNIT ACCESSION NO

11 TITLE (Include Security Classification)

Analysis and Mitigation of Optical Turbulence Effects

12 PERSONAL AUTHOR(S)
Charles L. Rino and Angela Regalia

13a. TYPE OF REPORT	13b TIME COVERED	14. DATE OF REPORT (Year, Month, Day)	15. PAGE COUNT
Final Report	FROM 2/1/90 TO 2/28/91	June 1991	42

16 SUPPLEMENTARY NOTATION Task was performed under a Scientific Services Agreement issued by Battelle, Research Triangle Park Office, 200 Park Drive, P.O. Box 12297, Research Triangle Park, NC 27709

17 COSATI CODES			18 SUBJECT TERMS (Continue on reverse if necessary and identify by block number)
FIELD	GROUP	SUB-GROUP	Optical Imaging Propagation Models Atmospheric Turbulence

19 ABSTRACT (Continue on reverse if necessary and identify by block number)

This document describes a consistently formulated propagation model for systems-oriented predictive codes. Simple models for the mutual coherence function of plane, spherical, and beam waves are developed. The results are given in terms of a path-integrated phase structure function based on Shkarofsky's approximation to the Kolmogorov model. A scheme for approximating the short-term mutual coherence function by approximating the phase structure function is developed. To provide a more quantitative measure of the recoverable degradation in an image, the instantaneous autocorrelation function for a refocused beam was simulated by using a phase-screen model. The results show that the short-term and long-term coherence measures are not linearly related. The difference is attributed to amplitude scintillation, which is not comprehended in phase reconstruction schemes.

20 DISTRIBUTION/AVAILABILITY OF ABSTRACT ☐ UNCLASSIFIED/UNLIMITED ☒ SAME AS RPT. ☐ DTIC USERS	21 ABSTRACT SECURITY CLASSIFICATION SAR
22a NAME OF RESPONSIBLE INDIVIDUAL MARIE RICHARDSON	22b TELEPHONE (Include Area Code) 505/678-2335 — 22c OFFICE SYMBOL SLCAS-MT-P

DD FORM 1473, 84 MAR — 83 APR edition may be used until exhausted. All other editions are obsolete. — SECURITY CLASSIFICATION OF THIS PAGE

Contents

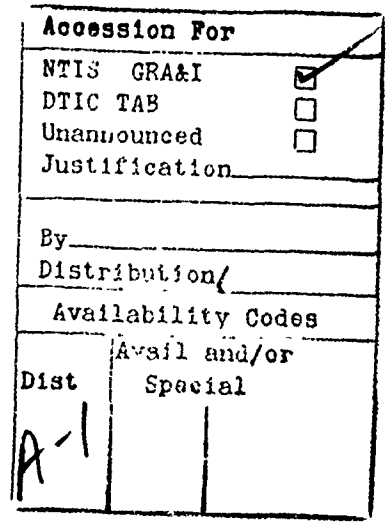

List of Figures

List of Tables

I INTRODUCTION

The U. S. Army Atmospheric Sciences Laboratory (ASL) maintains a systems-level code, IMTURB1, which is used to calculate propagation statistics for optical systems operating within the atmospheric boundary layer. The code contains an environment module and a propagation module. The environment module estimates the height-dependent turbulence level, the inner scale, and the outer scale as a function of meteorological variables. The propagation module uses the environmental parameters to predict the effects of propagation along extended paths within the turbulent region. The propagation model is based on a 1976 propagation code developed by Fried [1]. The basic parameters computed are (1) the log-amplitude variance, (2) the receiver coherence diameter for long- and short-term averages, (3) the isoplanatism effective path length, and (4) the scintillation averaging length [2].

Fried's model is based on the Rytov approximation, which formally restricts the results to small amplitude fluctuations. Nonetheless, the Rytov approximation is attractive because the propagation parameters can be computed in terms of comparatively simple path integrals. Over the past few decades, however, considerable progress has been made in the theory of wave propagation in random media, particularly under the narrow-angle scatter approximation. Thus, it is no longer necessary to accept the limitations of the Rytov approximation. Indeed, the linear systems approach to modeling imaging systems leads to image degradation measures that are expressed in terms of the mutual coherence function, which is amenable to exact evaluation. The linear systems model is reviewed in the appendix to this report.

The report proper describes a new propagation module that will allow the IMTURB1 code to accommodate essentially unrestricted propagation disturbance levels, while preserving the compact path-integral formulation. In work performed under a previous contract, the Shkarofsky spectral density function model was used to derive an analytic form for the phase structure function that retains explicit inner and outer scale cutoff parameters [3]. This provides an efficient method for computing the complete mutual coherence function (MCF) in place of the single-parameter characterization that is currently used in the IMTURB1 model. For plane and spherical waves this is easily done because the MCF admits a simple analytic characterization in terms of a path integral over the phase structure function. For beam waves, the corresponding path integral is nested in a two-dimensional integral that must be evaluated numerically or approximated. An approximation proposed by Ishimaru is used for the proposed propagation module.

To provide a consistent framework for computing the effects of long and short integration times, a scheme proposed by Fante has been implemented in which the low-frequency spectral contribution is removed before the structure function is computed.

Thus, the same basic theoretical/computational framework can be used for all the propagation parameters. The short-term results are incorporated as correction factors to the long-term structure function with the necessary numerical integrations approximated by a set of polynomial functions. This allows efficient computation within the propagation module.

For completeness we have repeated some earlier material describing the general solution to the parabolic wave equation for the mutual coherence function (Section II) and the Shkarofsky spectral form that is used to model the phase structure function (Section III). We then review the specific forms of the mutual coherence function that are proposed for plane, spherical, and beam waves (Section IV). Section V describes the modifications for short integration times. The results form a complete and consistently formulated propagation module, which can be integrated into the IMTURB code framework.

To provide some guidelines for interpreting the theoretical results, a numerical simulation has been implemented as was recently done by Martin and Flatté [4]. To translate the results to imaging systems, however, the simulated beam wave field was refocused to a point. Several measures of the averaged refocused beam degradation were then computed to evaluate both short-term and long-term beam degradations. These results are described in Section VI.

II BACKGROUND

Propagation of light in the atmospheric boundary layer is governed by the parabolic wave equation

$$2ik\frac{\partial U'(\mathbf{r})}{\partial z} + \nabla_\perp^2 U'(\mathbf{r}) + k^2\epsilon_1(\mathbf{r})U'(\mathbf{r}) = 0, \tag{1}$$

where

$$u(\mathbf{r}) = U'(\mathbf{r})\exp\{ikz\}. \tag{2}$$

For scintillation studies, one typically assumes that the relative permittivity, ϵ_1, consists of a locally invariant component plus a purely random perturbation; however, it is instructive to accommodate an explicit secular variation, whereby

$$\epsilon_1 = \bar{\epsilon}_1 + \delta\epsilon, \tag{3}$$

with $\bar{\epsilon}_1$ representing the slowly varying background component. As a first step in isolating the effects of $\bar{\epsilon}_1$, let

$$U'(\mathbf{r}) = U(\mathbf{r})\exp\{i\psi(\mathbf{r})\}. \tag{4}$$

One approach attempts to identify ψ as a ray-optics component, in which case it has both real and imaginary components as does the diffractive component U. It is simpler, however, to *define* ψ as the solution to

$$\frac{\delta\psi(\mathbf{r})}{\partial z} = k^2\bar{\epsilon}_1(\mathbf{r})\psi(\mathbf{r}). \tag{5}$$

By substituting (3) and (4) into (1) and using (5), it is readily shown that

$$2ik\frac{\partial U}{\partial z} = \nabla_\perp^2 U - (\nabla_\perp^2\psi)U = k^2\delta\epsilon U. \tag{6}$$

Now assume that $|\nabla_\perp^2\psi| << |\nabla_\perp^2 U/U|$, whereby the ψ-dependent term in (6) can be neglected, and U itself satisfies the parabolic wave equation.

It follows that solutions to the parabolic wave equation based only on the homogeneous random field $\delta\epsilon$ omit the effects of slow phase variation induced by $\bar{\epsilon}_1$. In an imaging system, this phase variation will cause a small, slowly varying displacement of the image. Such effects, however, are often attributed to the low-frequency component of the homogeneous turbulence. Indeed Fried has used the Rytov phase to compute the mean-square linear slope for homogeneous turbulence as a measure of the average image displacement. Based on the results presented in Section VI, however, we believe that this component is too small to account for the observed beam wander for weak

propagation disturbances. To properly interpret the beam wander, the inhomogeneous contribution must be modeled separately and incorporated explicitly as in (4).

Either way, the most important quantity for predicting the systems effects of atmospheric turbulence is the mutual coherence function, which is defined as

$$\Gamma(\Delta\rho; z, \rho_c) = <U(\rho_c + \Delta\rho/2, z)U^*(\rho_c - \Delta\rho/2, z)>, \tag{7}$$

where the angle brackets denote ensemble averaging, $\Delta\rho = \rho' - \rho$, and $\rho_c = (\rho + \rho')/2$. Under conditions that are readily satisfied for most applications, it can be shown that Γ satisfies the differential equation

$$\left\{2ik\frac{\partial}{\partial z} + (\nabla^2_{\perp_1} - \nabla^2_{\perp_2}) + \frac{ik^3}{2}(A(0) - A(\Delta\rho))\right\}\Gamma(\Delta\rho; z, \rho_c) = 0, \tag{8}$$

where $A(\Delta\rho)$ is the autocorrelation function of the refractive index perturbation. Thus, insofar as the scattering medium is concerned, it is only necessary to model the structure function $D_\epsilon(\Delta\rho) = 2(A(0) - A(\Delta\rho))$. Closed-form solutions can be obtained for point sources and the limiting case of plane waves. Good approximations are also available for beams as summarized in Section IV.2.

III PHASE STRUCTURE FUNCTION

III.1 General Results

As discussed in Section II, the solutions to the parabolic wave equation for the complex moments of U can be formulated in terms of the phase structure function. Thus, the phase structure function is fundamental in any propagation modeling effort. Consider a rectangular coordinate system with the z axis along the direction of propagation. The phase path integral for a distance l_p is given as

$$\delta\phi = k \int_0^{l_p} \delta\epsilon(\rho, z)\, dz. \tag{9}$$

The phase autocorrelation function can be computed from (9) as

$$<\delta\phi\delta\phi'>= k^2 \int_0^{l_p} \int_0^{l_p} <\delta\epsilon(\rho, z)\delta\epsilon(\rho', z')>\ dz dz'. \tag{10}$$

For homogeneous statistics,

$$<\delta\epsilon\delta\epsilon'>= B_\epsilon(\Delta\rho, \Delta z). \tag{11}$$

By using (11) and performing a straightforward change of variables in (10), one obtains

$$<\delta\phi\delta\phi'>= k^2 l_p \int_{l_p}^{l_p} (1 - |\Delta z|/l_p)\, B_\epsilon(\Delta\rho, \Delta z)\, d\Delta z. \tag{12}$$

For almost all applications, the correlation distance along z is small compared to l_p, in which case the integral in (12) can be replaced by

$$A(\Delta\rho) = \int_{-\infty}^{\infty} B_\epsilon(\Delta\rho, \Delta z)\, d\Delta z. \tag{13}$$

Let us now define the spectral density function (SDF) as

$$\bar{\Phi}(\mathbf{K}, k_z) = \frac{1}{(2\pi)^3} \iiint B_\epsilon(\Delta\rho, \Delta z) \exp\{-i(\mathbf{K}\cdot\Delta\rho + k_z\Delta z)\}\, d\Delta\rho dz. \tag{14}$$

The overbar is used to denote SDFs normalized as in (14) rather than as in the alternative definition that places the $(2\pi)^3$ term in the denominator of the complementary spectral integral. If the SDF is isotropic, it is readily shown that

$$A(\Delta\rho) = (2\pi)^2 \int_0^{\infty} J_0(K\Delta\rho)\bar{\Phi}_\epsilon(K) K\, dK. \tag{15}$$

The refractive index n is related to ϵ as

$$n = \sqrt{\frac{\epsilon}{\epsilon_0}} = \bar{n}\sqrt{1+\epsilon_1} \approx \bar{n}\left(1+\frac{\epsilon_1}{2}\right). \tag{16}$$

It follows that $4R_n = R_\epsilon$. Thus, the structure function for the refractive index is given as

$$\begin{aligned} D_n(\Delta\rho) &= \frac{1}{2}(A(0) - A(\Delta\rho)) \\ &= 2\pi^2 \int_0^\infty (1 - J_0(K\Delta\rho))\bar{\Phi}_\epsilon(K) K\, dK. \end{aligned} \tag{17}$$

It is convenient to define a spectral shape function $Q(q)$ such that

$$\int_0^\infty Q(q) q^2 \frac{dq}{2\pi^2} = 1. \tag{18}$$

With

$$\bar{\Phi}_n(K) = <\delta n^2> \frac{Q(q)}{(2\pi)^3}, \tag{19}$$

it follows that

$$\iiint \bar{\Phi}_n(\mathbf{k})\, d\mathbf{k} = <\delta n^2>. \tag{20}$$

We note that the structure function occurs naturally in gaussian random field theory. Let $U(\rho) = \exp\{i\delta\phi(\rho)\}$, where $\delta\phi$ is a gaussian process. It follows from the properties of gaussian variables that

$$\begin{aligned} <UU'^*> &= \exp\{-\frac{1}{2} <(\delta\phi(\rho) - \delta\phi(\rho'))^2>\} \\ &= \exp\{-k^2 l_p D_n(\Delta\rho)\}. \end{aligned} \tag{21}$$

Indeed, (21) is the mutual coherence function for a plane wave propagating in a homogeneous random medium; however, this occurs because the diffraction effects that modulate the complex diffracted wave field average to unity in the average coherence computation.

III.2 Power-law Spectral Models

The modified Kolmogorov spectrum is defined in terms of the structure constant C_n^2 and the inner l_0 and outer L_0 scale sizes as

$$\bar{\Phi}_n(k) = 0.033 C_n^2 (k_L^2 + k^2)^{-11/6} \exp\{-k^2/k_m^2\}, \tag{22}$$

where

$$k_m = 5.92/l_0 \tag{23}$$

$$k_L = 1/L_0. \tag{24}$$

The full wave vector is conveniently specified in terms of its transverse and axial components as $\mathbf{k} = (\mathbf{K}, k_z)$. Bold-face symbols indicate vectors. The magnitudes of the vector components will be indicated by the corresponding ordinary symbol. A problem with (22) is that it does not admit a closed form for $A(\Delta\rho)$. A more convenient form was developed by Shkarofsky [5]. It will be used in a slightly modified form, which is summarized in Table 2 of [6], namely,

$$Q(q) = (2\pi\alpha_s\alpha_L)^{3/2}\sqrt{1+\frac{(\alpha_L q)^2}{2}}^{-(\nu+1/2)}\frac{K_{\nu+1/2}\left(2\frac{\alpha_s}{\alpha_L}\sqrt{1+\frac{(\alpha_L q)^2}{2}}\right)}{K_{\nu-1}\left(2\frac{\alpha_s}{\alpha_L}\right)}, \tag{25}$$

where $K_\nu(x)$ is the modified Bessel function of fractional order. It will also be convenient to define

$$\begin{aligned}\kappa &= \int_0^\infty qQ(q)\frac{dq}{2\pi} \\ &= \sqrt{2\pi\alpha_s\alpha_L}\frac{K_{\nu-1/2}\left(2\frac{\alpha_s}{\alpha_L}\right)}{K_{\nu-1}\left(2\frac{\alpha_s}{\alpha_L}\right)}.\end{aligned} \tag{26}$$

It can be shown that

$$\begin{aligned}R(y) &= A(\Delta\rho)/A(0) \\ &= \int_0^\infty qJ_0(qy)Q(q)\,dq/\int_0^\infty qQ(q)\,dq \\ &= \sqrt{1+\frac{y^2}{2\alpha_s^2}}^{\nu-1/2}\frac{K_{\nu-1/2}\left(2\frac{\alpha_s}{\alpha_L}\sqrt{1+\frac{y^2}{2\alpha_s^2}}\right)}{K_{\nu-1/2}\left(2\frac{\alpha_s}{\alpha_L}\right)}.\end{aligned} \tag{27}$$

Thus, Q, R or Φ_n and A have self-similar Fourier transforms.

For small values of x, $K_{\nu-1}(2x) \approx \frac{1}{2}\Gamma(\nu-1)(\alpha_s/\alpha_L)^{-\nu+1}$. For all applications of interest, $\alpha_s/\alpha_L << 1$. Thus, for $q << 1/\alpha_s$ (25) simplifies to

$$Q(q) \approx \frac{8\pi^{3/2}(\alpha_L/\sqrt{2})^{2(1-\nu)}\Gamma(\nu+1/2)}{\Gamma(\nu-1)}\left(\frac{2}{\alpha_L^2}+q^2\right)^{-\nu-1/2}. \tag{28}$$

Equation (28) can be put in the same form as (22) if (28) is first divided by $(2\pi)^3$ to maintain consistent 2π conventions. We then let $\alpha_L = \sqrt{2}L_0$ and

$$<\delta n^2> \frac{(L_0)^{2(1-\nu)}\Gamma(\nu+1/2)}{\pi^{3/2}\Gamma(\nu-1)} = 0.033C_n^2, \tag{29}$$

or

$$<\delta n^2> = \frac{\pi^{3/2}\bar{C}_s\Gamma(\nu-1)}{\Gamma(\nu+1/2)q_0^{2\nu-2}}, \tag{30}$$

where $q_0 = L_0^{-1}$ and $\bar{C}_s = 0.033C_n^2$. By noting that $A(0) = \kappa <\delta^2>$, we can obtain a consistent expression for $D_\epsilon(y)$ or $D_n(y)$. The complete model is summarized in Table 1 in terms of the basic parameters C_n^2, l_0, L_0, and the 11/3 power, which corresponds to $\nu = 4/3$.

Figure 1 shows a comparison of the Kolmogorov and Shkarofsky spectral forms for a fixed inner scale of 1 cm and a typical outer scale range. The Shkarofsky model was evaluated from Table 1. Standard subroutines were used to evaluate the Bessel and gamma functions. It can be seen that significant differences occur only in the regime of the inner scale cutoff. Because the detailed mathematical form in the dissipation regime is not known precisely, these differences are unimportant. Figure 2 shows the Shkarofsky form of the structure function as summarized in Table 1. Although the Shkarofsky form is convenient for modeling, it can be unwieldy for analytic computation. Thus, the approximations are often used.

In the inertial subrange $L_0 < q < l_0$, $\bar{\Phi}_n$ has the power-law form $\bar{C}_s q^{-11/3}$. By carefully evaluating $\lim_{L_0\to\infty} D_n(y)$ it can be shown that the structure function admits the complementary power-law form

$$D_n(y) \approx \frac{4\pi^2\bar{C}_s\Gamma(3/2-\nu)}{\Gamma(\nu+1/2)(2\nu-1)2^{2\nu-2}}y^{2\nu-1}. \tag{31}$$

Note that (31) does not depend on L_0. Carrying out a Taylor series expansion of $D_n(y)$ for small y, using (31) for intermediate y, and the saturation value of $D_n(y)$ for large y, it follows that

$$D_n(y) = \begin{cases} 4\pi^2\bar{C}_s\frac{\Gamma(3/2-\nu)l_0^{2\nu-3}}{\Gamma(\nu-1/2)2^{2\nu-1}}y^2 & y < l_0 \\ 4\pi^2\bar{C}_s\frac{\Gamma(3/2-\nu)}{\Gamma(\nu+1/2)(2\nu-1)2^{2\nu-2}}y^{2\nu-1} & l_0 < y < L_0 \\ 4\pi^2\bar{C}_s\frac{\Gamma(\nu-1/2)}{\Gamma(\nu+1/2)q^{2\nu-1}} & y > L_0 \end{cases} . \tag{32}$$

Evaluating the coefficients for the Kolmogorov value $\nu = 4/3$, we obtain

$$D_n(y) \approx \begin{cases} 2.024 C_n^2 \frac{y^2}{l_0^{1/3}} & y < l_0 \\ 2.913 C_n^2 y^{5/3} & l_0 < y < L_0 \\ 1.563 C_n^2 L_0^{5/3} & y > L_0 \end{cases} . \tag{33}$$

The asymptotic and saturation forms of (33) are identical to the corresponding forms from (20-78) in Ishimaru [7] when allowance is made for the factor of 2 difference between $A(0) - A(y)$ and $D_n(y)$ from (17). The small y form given by Ishimaru is about 62% larger, which reflects the differences between the Shkarofsky and Kolmogorov forms. Equation (33) is plotted in Figure 3. It can be seen that the quadratic and asymptotic regimes are narrowly confined, and results based on these approximations must be restricted accordingly.

Table 1. Summary of Shkarofsky Form of Modified Kolmogorov Spectrum.

Shkarofsky Model $\nu = 4/3$

$$\bar{\Phi}_n(q) = <\delta n^2> \frac{Q(q)}{(2\pi)^3}$$

$$Q(q) = (2\pi\alpha_s\alpha_L)^{3/2}\sqrt{1+\frac{(\alpha_L q)^2}{2}}^{-(\nu+1/2)} \frac{K_{\nu+1/2}\left(2\frac{\alpha_s}{\alpha_L}\sqrt{1+\frac{(\alpha_L q)^2}{2}}\right)}{K_{\nu-1}\left(2\frac{\alpha_s}{\alpha_L}\right)}$$

$$D_n(y) = \frac{4\pi^2\bar{C}_s\Gamma(\nu-1/2)}{\Gamma(\nu+1/2)}\left[\frac{1-R(y)}{q_0^{2\nu-1}}\right] \quad \bar{C}_s = 0.033C_n^2$$

$$R(y) = \sqrt{1+\frac{y^2}{2\alpha_s^2}}^{\nu-1/2} \frac{K_{\nu-1/2}\left(2\frac{\alpha_s}{\alpha_L}\sqrt{1+\frac{y^2}{2\alpha_s^2}}\right)}{K_{\nu-1/2}\left(2\frac{\alpha_s}{\alpha_L}\right)}$$

$$<\delta n^2> = \frac{\pi^{3/2}\bar{C}_s\Gamma(\nu-1)}{\Gamma(\nu+1/2)q_0^{2\nu-2}} \quad q_0 = L_0^{-1}$$

$$\alpha_L = \sqrt{2}L_0 \quad \alpha_s = l_0/\sqrt{2}$$

$$C(y) = <\delta n^2> R(y)$$

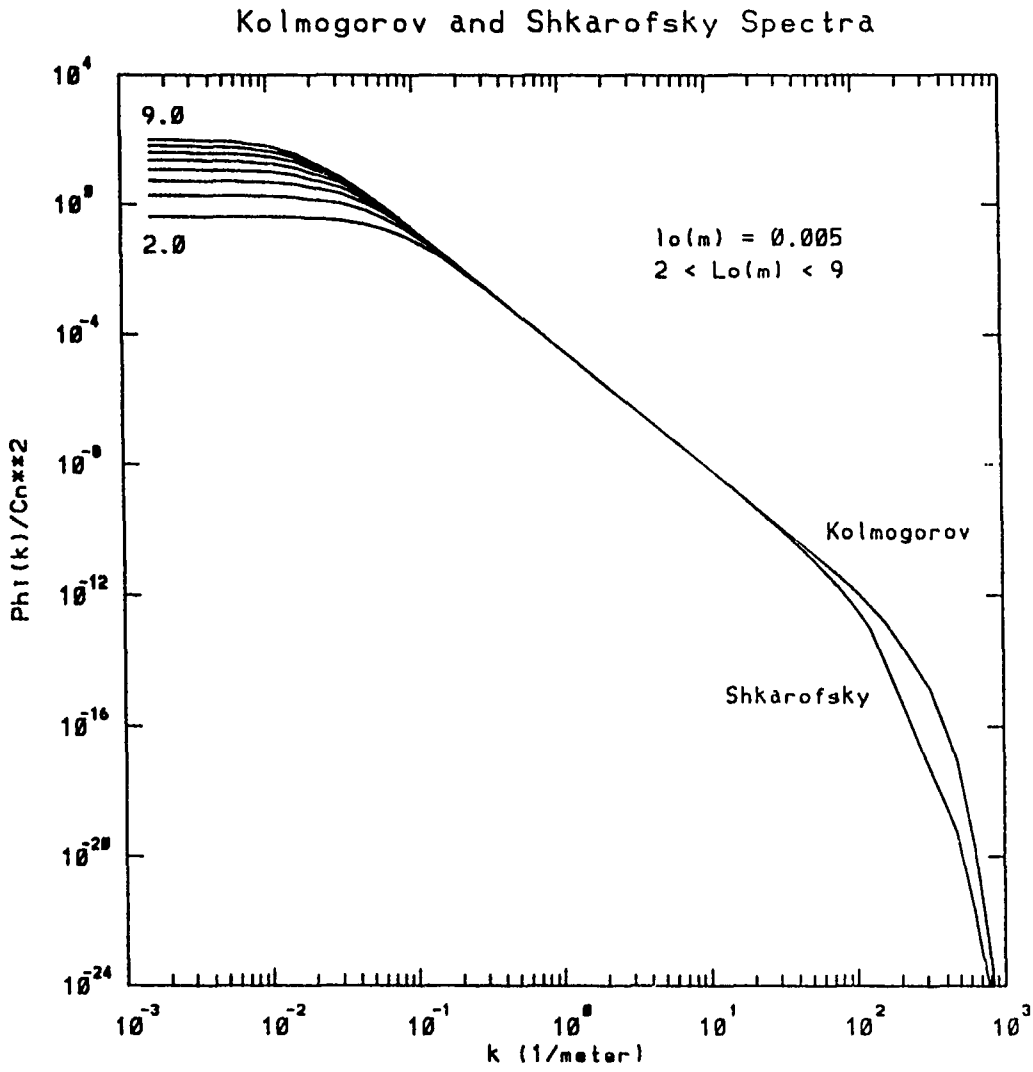

Figure 1. Comparison of Kolmogorov and Shkarofsky spectral models.

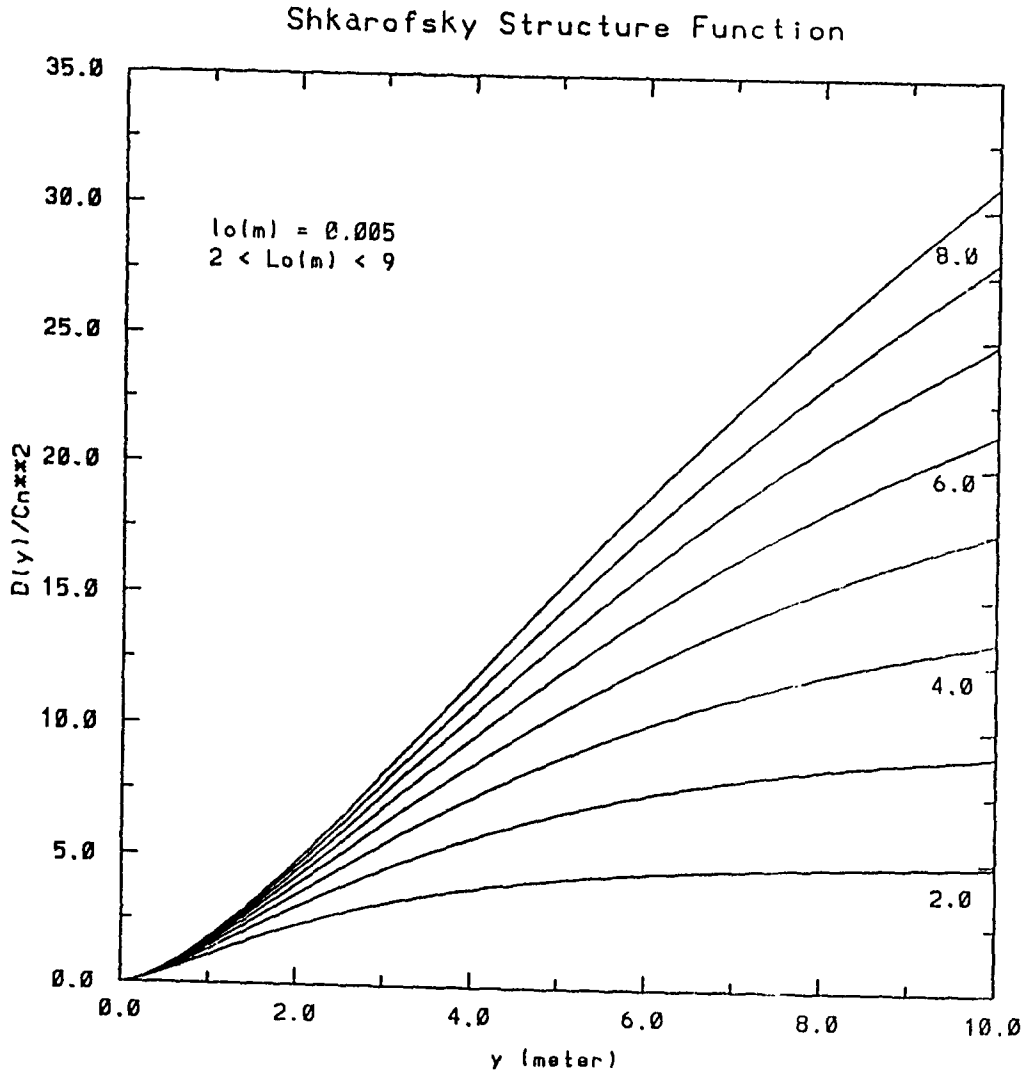

Figure 2. Shkarofsky form of structure function.

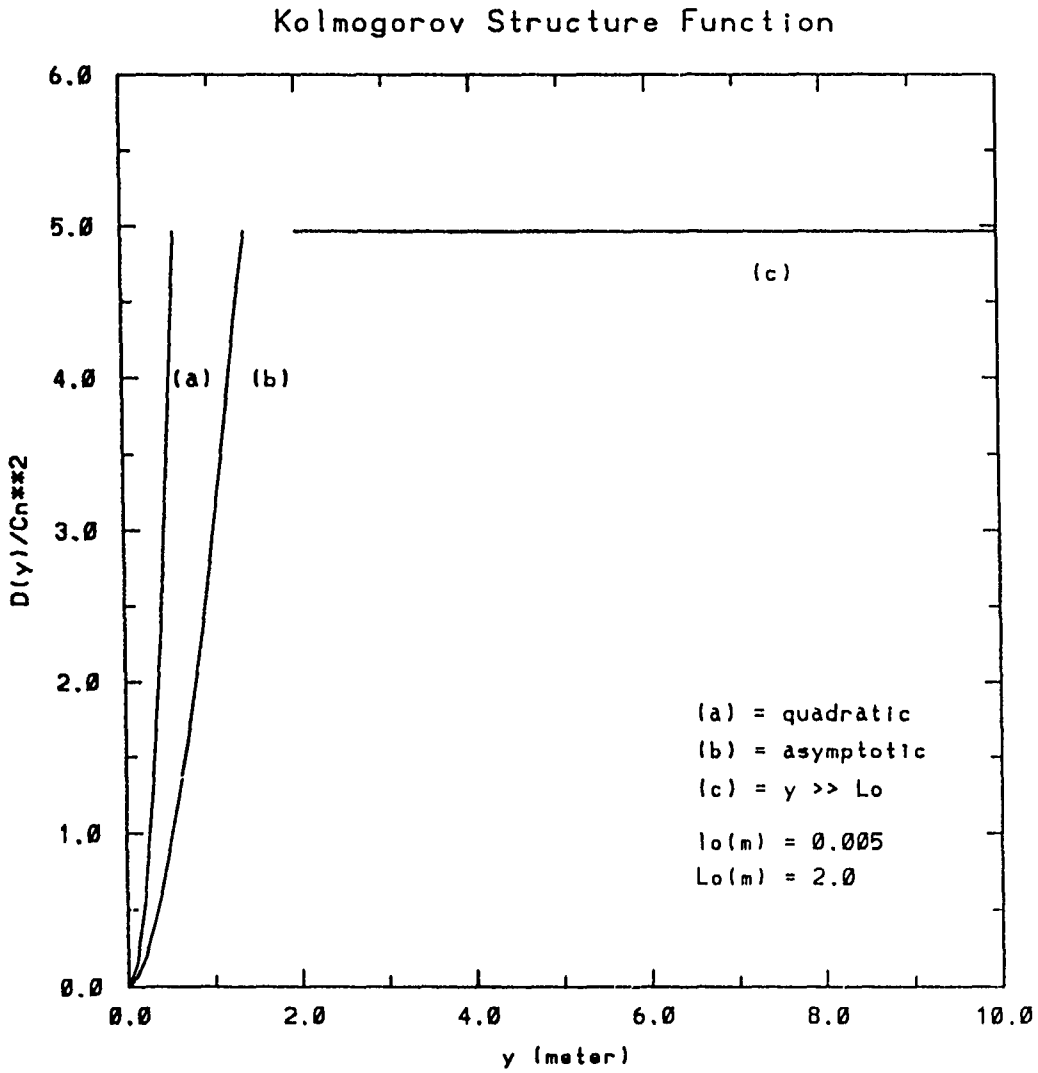

Figure 3. Approximate forms for structure function regimes.

IV MUTUAL COHERENCE FUNCTION

The results summarized in this section are taken from Chapter 20-6 of Ishimaru [7], where detailed derivations and an extensive bibliography can be found. As noted in Section II, all solutions to the differential equation (8) derive their dependence on the propagation medium from the structure function for the refractive index $D_n(y)$, where y represents the magnitude of $\Delta\rho$. In a plane normal to the propagation direction, the structure function is isotropic.

The receiver coherence diameter, r_0, which is defined as the path separation in the receiver plane over which the spatial coherence of the complex field decreases by the factor e^{-1}, is a useful parameter for evaluating the effects of atmospheric turbulence. In the current version of IMTURB1, an approximation to r_0 is obtained by integrating the local asymptotic value; however, with the Shkarofsky model it is a simple matter to compute the exact coherence function.

IV.1 Plane and Spherical Waves

For a plane wave, the mutual coherence function is position-invariant and has already been given by (21). For a spherical wave emanating from the origin of the reference coordinate system, it can be shown that

$$\Gamma(\Delta\rho;\rho_c,z)=\frac{1}{z^2}\exp\{i\frac{k}{z}\rho_c\cdot\Delta\rho-H(\Delta\rho;z)\},\tag{34}$$

where

$$H(\Delta\rho;z)=\frac{k^2}{2}\int_0^z D_\epsilon(yz'/z)\,dz'.\tag{35}$$

There is a deterministic dependence on position relative to the source that can be important. The spreading loss is given by the z^{-2} dependence, but this factor is conveniently absorbed in the gain factors for the optical system of interest. The most important turbulence effect for spherical waves is the variation in the effective coherence scale along the integration path—the shower-glass effect. Regions of very high turbulence near the source are not as troublesome as regions of moderate turbulence further along the path.

IV.2 Beam Waves

The fundamental quantity of interest is the complex wavefield $u(\mathbf{r})$, but for narrow-angle scatter it is convenient to introduce the modified wavefield

$$U(\rho,z)=u(\mathbf{r})\exp\{-ikz\}.\tag{36}$$

For a beam wave,

$$U(\boldsymbol{\rho},0) = \exp\{-\frac{1}{2}k\alpha\rho^2\}, \tag{37}$$

which has the two-dimensional Fourier transform

$$U(\mathbf{K},0) = \frac{\pi}{k\alpha}\exp\{-\frac{K^2}{4k\alpha}\}. \tag{38}$$

Beyond the $z = 0$ plane,

$$\begin{aligned} U(\boldsymbol{\rho},z) &= \iint U(\mathbf{K},0)\exp\{ik(g(K)-1)z\}\exp\{i\mathbf{K}\cdot\boldsymbol{\rho}\}\frac{d\mathbf{K}}{(2\pi)^2} \\ &\approx \frac{1}{1+i\alpha z}\exp\{-\frac{k\alpha}{2}\frac{\rho^2}{1+i\alpha z}\}. \end{aligned} \tag{39}$$

To evaluate the integral, the narrow-angle scatter approximation $g(K) = \sqrt{1-(K/k)^2} \approx 1-(K/k)^2/2$ was used. It follows that

$$|U(\boldsymbol{\rho},z)|^2 = (W_0/W(z))^2\exp\{-2\rho^2/W^2(z)\}, \tag{40}$$

where

$$W^2(z) = W_0^2[(1-\alpha_i z)^2 + (\alpha_r z)^2]. \tag{41}$$

Ishimaru sets $\alpha_r = 2/(kW_0^2)$ and $\alpha_i = 1/R_0$, whereby $W(z)$ achieves a minimum at $z \approx \pm 1/R_0$. Thus, the beam wavefield, which has initial size W_0, either converges to a minimum at $z = 1/R_0$ (focused) or diverges from a fictitious point at $z = -1/R_0$ (unfocused).

Under the conditions of narrow-angle scatter and small local perturbations, the MCF of an arbitrary wavefield admits the integral representation

$$\begin{aligned} \Gamma(\Delta\boldsymbol{\rho},\boldsymbol{\rho}_c,z) &= \iint \Gamma_0(\Delta\boldsymbol{\rho} - z\mathbf{K}_d/k;\mathbf{K}_d;0)\exp\{i\mathbf{K}_d\cdot\boldsymbol{\rho}_c\} \\ &\quad \times \exp\{-H(\Delta\boldsymbol{\rho} - z\mathbf{K}_d/k;\mathbf{K}_d)\}\,d\mathbf{K}_d, \end{aligned} \tag{42}$$

where

$$\Gamma_0(\boldsymbol{\rho}_d;\mathbf{K}_d;0) = \frac{1}{(2\pi)^2}\iint \Gamma_0(\boldsymbol{\rho}_d,\boldsymbol{\rho}_c;0)\exp\{-i\mathbf{K}_d\cdot\boldsymbol{\rho}_c\}\,d\boldsymbol{\rho}_c \tag{43}$$

and

$$H(\Delta\boldsymbol{\rho};\mathbf{K}_d) = -\frac{k^2}{2}\int_0^z D_n(\Delta\boldsymbol{\rho} + z'\mathbf{K}_d/k)\,dz'. \tag{44}$$

The quantity $\Gamma_0(\Delta\boldsymbol{\rho},\boldsymbol{\rho}_c,0)$ represents the MCF of the incident wavefield at $z = 0$ in terms of the sum variable $\boldsymbol{\rho}_c = (\boldsymbol{\rho}_1+\boldsymbol{\rho}_2)/2$ and the difference variable $\Delta\boldsymbol{\rho} = \boldsymbol{\rho}_2 - \boldsymbol{\rho}_1$.

For a plane wave, $\Gamma_0(\boldsymbol{\rho}_d, \boldsymbol{\rho}_c, 0) = 1$, which implies that

$$\Gamma_0(\boldsymbol{\rho}_d; \mathbf{K}_d, 0) = \delta(\mathbf{K}_d) \tag{45}$$

independent of $\boldsymbol{\rho}_d$. Substituting (45) into (42) gives

$$\Gamma(\Delta\boldsymbol{\rho}, \boldsymbol{\rho}_c, z) = \exp\{-\frac{k^2}{2}\int_0^z D_n(\Delta\boldsymbol{\rho})\, dz'\}, \tag{46}$$

which is independent of $\boldsymbol{\rho}_c$. The $\Delta\boldsymbol{\rho}$ dependence of the final result comes from $H(\Delta\boldsymbol{\rho}; 0)$.

For a spherical wave,

$$U_0(\boldsymbol{\rho}, z) = \frac{1}{z}\exp\{ik\rho^2/(2z)\}, \tag{47}$$

so that

$$\Gamma_0(\Delta\boldsymbol{\rho}, \boldsymbol{\rho}_c; z) = \frac{1}{z}\exp\{ik\boldsymbol{\rho}_c \cdot \Delta\boldsymbol{\rho}/z\}. \tag{48}$$

It is readily shown that

$$\Gamma(\boldsymbol{\rho}_d; \mathbf{K}_d, z) = \frac{1}{z^2}\delta(\mathbf{K}_d - k\boldsymbol{\rho}_d/z). \tag{49}$$

Taking the limit as $z \to 0$, it follows that

$$\Gamma(\boldsymbol{\rho}; \mathbf{K}_k; 0) = \frac{1}{k^2}\delta(\boldsymbol{\rho}_d). \tag{50}$$

Substituting (50) into (42) as before gives

$$\Gamma(\Delta\boldsymbol{\rho}, \boldsymbol{\rho}_c; z) = \frac{\exp\{ik\Delta\boldsymbol{\rho} \cdot \boldsymbol{\rho}_c/z\}}{z^2}\exp\{-\frac{k^2}{2}\int_0^z D_n(\Delta\boldsymbol{\rho}z'/z)\, dz'\}. \tag{51}$$

The leading term in (51) is the MCF for the spherical wave source.

For a beam wave, it follows from (37) that

$$\Gamma_0(\Delta\boldsymbol{\rho}, \boldsymbol{\rho}_c, 0) = \exp\{-k[\alpha_r(\rho_c^2 + \Delta\rho^2/4) + i\alpha_i\boldsymbol{\rho}_c \cdot \Delta\boldsymbol{\rho}]\}. \tag{52}$$

Substituting (52) into (43) it follows by direct computation that

$$\Gamma_0(\boldsymbol{\rho}_d; \mathbf{K}_d; 0) = \frac{1}{4\pi k\alpha_r}\exp\{-k\alpha_r\rho_d^2/4 - [\mathbf{K}_d + k\alpha_i\boldsymbol{\rho}_d]^2/(4k\alpha_r)\}. \tag{53}$$

Furthermore,

$$\lim_{\alpha_r \to 0}\Gamma_0(\boldsymbol{\rho}_d; \mathbf{K}_d; 0) = \delta(\mathbf{K}_d + k\alpha_i\boldsymbol{\rho}_d). \tag{54}$$

If $\alpha_i = 0$, we recover the plane-wave result. At the other extreme of large α_i we have

$$\lim_{\alpha_r \to 0}\Gamma_0(\boldsymbol{\rho}_d; \mathbf{K}_d; 0) \approx \frac{1}{(k\alpha_i)^2}\delta(\boldsymbol{\rho}_d). \tag{55}$$

IV.3 Small α_r Approximation

For the moment, let us assume that we are free to make α_r as small as we like. In that case the integral of (42) with Γ_0 defined by (53) can be evaluated by the saddle point method. After some straightforward manipulations we find that

$$\begin{aligned}\Gamma(\Delta\rho;\rho_c;z) &\approx (W_0/W(z))^2 \exp\{b^2/(4a) - c\Delta\rho^2\} \\ &\quad \times \exp\{-\frac{k^2}{2}\int_0^z D_n(\Delta\rho + (z'-z)\mathrm{K}_d^s/k)\,dz'\}, \qquad (56)\end{aligned}$$

where

$$a = \frac{1}{4k\alpha_r}((1-\alpha_i z)^2 + (\alpha_r z)^2) \approx \frac{(1-\alpha_i z)^2}{4k\alpha_r}, \qquad (57)$$

$$\mathbf{b} = \frac{1}{4k\alpha_r}\left[2k(\alpha_i(1-\alpha_i z) - \alpha_r^2 z)\Delta\rho + 4ik\alpha_r\rho_c\right] \approx \frac{\alpha_i(1-\alpha_i z)}{2\alpha_r}\Delta\rho, \qquad (58)$$

$$c = \frac{k}{4\alpha_r}(\alpha_r^2 + \alpha_i^2) \approx \frac{k\alpha_i^2}{4\alpha_r}, \qquad (59)$$

$$\mathrm{K}_d^s = -\mathrm{b}/(2a) \approx \frac{k\alpha_i\Delta\rho}{1-\alpha_i z}. \qquad (60)$$

Upon substituting the approximate forms of (57), (58), (59), and (60) into (56), the dependence on α_r cancels and the result implied by (54) is obtained. The accuracy of the saddle point method depends on

$$F(\mathrm{K}_d) = \exp\{-\frac{k^2}{2}\int_0^z D(\Delta\rho + (z'-z)(\mathrm{K}_d^s + \mathrm{K}_d)/k)\,dz'\} \qquad (61)$$

varying slowly over K_d regions such that $|\mathrm{K}_d| << 1/a$. A test of this condition can be made upon evaluating the integral in (56). The three MCF forms are summarized in Table 2.

Table 2. Summary of mutual coherence function forms.

Wave Type	$\Gamma(\Delta\,\boldsymbol{\rho};\boldsymbol{\rho}_c;z)$
Plane	$\exp\{-\frac{k^2}{2}\int_0^z D_n(\Delta\boldsymbol{\rho})\,dz'\}$
Spherical	$\frac{\exp\{ik\Delta\boldsymbol{\rho}\cdot\boldsymbol{\rho}_c/z\}}{z^2}\exp\{-\frac{k^2}{2}\int_0^z D_n(\Delta\boldsymbol{\rho}z'/z)\,dz'\}$
Beam	$(W_0/W(z))^2\exp\{b^2/(4a)-c\Delta\rho^2\}$ $\times\exp\{-\frac{k^2}{2}\int_0^z D_n(\Delta\boldsymbol{\rho}+(z'-z)\mathbf{K}_d^s/k)\,dz'\}$

IV.4 Intensity Statistics

The fourth-order moment of the complex field satisfies a known differential equation, which has received considerable attention over the past five years. Through numerical simulations, diagram methods, asymptotic expansions, and other techniques a detailed understanding has emerged, but the most general results cannot yet be encoded into simple formulas. For our purposes here, we shall restrict ourselves to single-frequency two-point correlations, which are the direct extension of the mutual coherence function analysis. For a single phase screen, it can be shown [8, 9] that the spatial wavenumber spectrum of the intensity is given by the integral

$$\Phi_I(\mathbf{K}) = \iint \exp\{-g(\xi,\mathbf{K}l_f^2)\}\cos(\mathbf{K}\cdot\xi)\,d\xi \tag{62}$$

where

$$g(\xi,\eta) = 8k^2 l_p \iint \Phi(\mathbf{q},0)\sin^2(\eta\cdot\mathbf{q}/2)\sin^2(\xi\cdot\mathbf{q}/2)\frac{d\mathbf{q}}{(2\pi)^2}, \tag{63}$$

$$l_f^2 = z/k, \tag{64}$$

and l_p is the path length as in Section III. The two-dimensional Fourier transform of (63) gives the intensity correlation function; however, we shall be mainly interested in the intensity moment

$$<I^2> - \iint \Phi_i(\mathbf{K})\frac{d\mathbf{K}}{(2\pi)^2}. \tag{65}$$

To remove the mean intensity, we define

$$\sigma_I^2 = <I^2> - 1, \tag{66}$$

which is strictly valid for plane waves but a good approximation for most applications.

If we substitute (22) into (63) and change variables, it can be shown that

$$g(\xi, \mathrm{K}l_f^2) = 8U \iint \frac{\exp\{-(q\gamma_m)^2\}}{[\gamma_L^2 + q^2]^{11/6}} \sin^2(\mathrm{K}l_f \cdot \mathrm{q}/2) \sin^2(\xi \cdot \mathrm{q}/(2l_f)) \frac{d\mathrm{q}}{(2\pi)^2}, \tag{67}$$

where

$$\begin{aligned} l_c' &= [k^2 l_p (0.033 C_n^2)]^{5/3} \\ U' &= (l_f/l_c')^{5/3} \\ \gamma_l &= k_l l_f \\ \gamma_m &= (k_m l_f)^{-1}. \end{aligned}$$

The main point here is that the behavior of the intensity statistics depends on two length parameters, l_f, which is the Fresnel radius, and l_c', which is close to the receiver coherence diameter, and two ratio parameters, γ_l and γ_m. If the parameters γ_l and/or γ_m become large, the influence of the corresponding scale size becomes small. The intensity statistics are well defined in the fractal limit where both the outer and inner scale sizes are respectively infinity and zero. For optical turbulence effects, however, the inner scale generally cannot be neglected.

For the moment, let us consider the fractal limit. If we replace l_c' with l_c such that $k^2 l_p D_n(l_c) = 1$, it can be shown [8] that

$$\sigma_I^2 \approx \frac{1}{2} U, \tag{68}$$

where

$$U = \frac{1}{2} k^2 l_p D_n(l_f). \tag{69}$$

The approximation is valid as long as $U << 1$. As U increases beyond this range, σ_I^2 will increase monotonically until it slightly exceeds unity and then will decrease to unity, its saturation value. The effects of the inner scale are shown in Figure 1 of Whitman and Beran [10]. The general effect is to shift the $\gamma_m = 0$ curve to the right and increase its amplitude. Simulations by Martin and Flatté [11] have shown that Whitman and Beran's calculations are about 15% too low, but the general shape is preserved. For modeling purposes, it would not be too difficult to fit a simple functional form to the

curves derived numerically or from simulations. For strong intensity fluctuation, we can use the saturation result

$$<II'> -1 \approx \exp\{-2H\}, \tag{70}$$

that is, we simply square the mutual coherence function. For weak intensity fluctuations approximations based on

$$\Phi_I(\mathrm{K}) \approx 4k^2 l_p \sin^2(K^2 l_f^2/2)\Phi_n(\mathrm{K})) \tag{71}$$

can be used.

V Slow and Fast Integration Times

In a turbulent flow field, structures of different sizes travel at different speeds. Nonetheless, the dominant propagation effects come from larger scale structures that are essentially frozen over the measurement integral. Thus, a long exposure image in the focal plane of an optical system will tend to measure the ensemble average of the angular deviation predicted by the MCF. Shorter sequential exposures tend to show sharper detail that rearrange themselves slowly in time. Assuming that these displacements come from the larger scale turbulent structures, one is motivated to define the short-term MCF as a high-pass filtered version of its long-term form. The concept is an old one, although it has no firm theoretical basis. The particular measure we have implemented was proposed by Fante [12].

For isotropic turbulence, the correlation function and spectral density functions are related by Hankel transforms. Thus, if

$$C(\Delta\rho) = 2\pi \int_0^\infty K J_0(K\Delta\rho)\bar{\Phi}_\epsilon(K)\,dK, \tag{72}$$

then

$$\bar{\Phi}_\epsilon(K) = \frac{1}{2\pi}\int_0^\infty \Delta\rho C(\Delta\rho)J_0(K\Delta\rho)\,d\Delta\rho. \tag{73}$$

It follows that

$$\begin{aligned} C_s(\Delta\rho) &= 2\pi\int_{K_0}^\infty K J_0(K\Delta\rho)\bar{\Phi}_\epsilon(K)\,dK \\ &= C(\Delta\rho) - 2\pi\int_0^{K_0} K J_0(K\Delta\rho)\bar{\Phi}_\epsilon(K)\,dK. \end{aligned} \tag{74}$$

Because we have an analytic form for $C(\Delta\rho)$, it is desirable to perform the filter operation in the spatial domain. It can be shown from (74) that

$$C_s(\Delta\rho) = C(\Delta\rho) - \int_0^\infty \Delta\rho' C(\Delta\rho')F(\Delta\rho,\Delta\rho')\,d\Delta\rho, \tag{75}$$

where

$$F(\Delta\rho,\Delta\rho') = K_0\int_0^\pi \frac{J_1(\sqrt{\Delta\rho^2+\Delta\rho'^2-2\Delta\rho\Delta\rho'\cos\theta})}{\sqrt{\Delta\rho^2+\Delta\rho'^2-2\Delta\rho\Delta\rho'\cos\theta}}\,\frac{d\theta}{2\pi}. \tag{76}$$

The short-term structure function can then be written as

$$D_s(\Delta\rho) = D_n(\Delta\rho) - 0.5(C_s(0) - C_s(\Delta\rho)). \tag{77}$$

The short-term correction to be applied to $D_n(\Delta\rho)$ to obtain $D_s(\Delta\rho)$ is obtained by interpolating a precalculated set of offset curves. Prior to computing the offset curves,

the structure functions are normalized to C_n^2, which effectively reduces the dependence on the structure constant to a scale factor. It was found that the dependence on the inner scale is very weak, so that a nominal value of .5 cm could be used. The remaining parameters are $\Delta\rho$, L_0, and K_0, which is expressed as a fraction of $2\pi/L_0$. The effect of changing K_0 is similar to changing L_0 itself. Figure 4 shows a family of five D_s curves for $K_0 = 0.1$, 0.25, 0.5, 2.0, and 3.0 times $2\pi/L_0$. As the fast cutoff wavenumber increases, the correlation at a fixed separation increases. This implies a sharper image, which may be disp'aced.

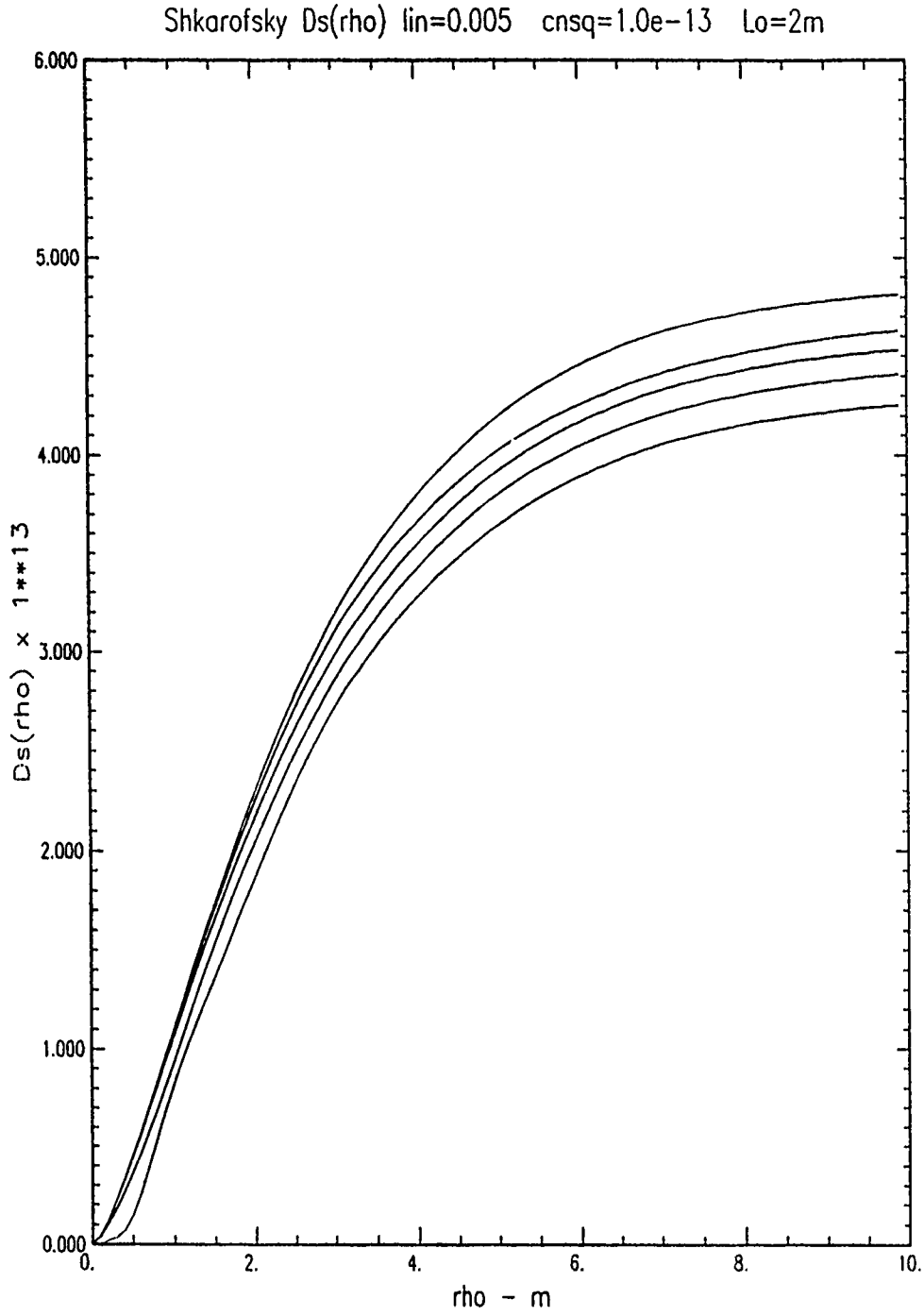

Figure 4. Structure function for fast integration times.

VI Simulation of Imaging in Turbulence

VI.1 Background

The IMTURB code provides quantitative system performance guidelines for imaging systems operating in the turbulent atmospheric boundary layer, but it is very difficult to design definitive validation tests for the model. Ideally, one would design experiments that combined channel diagnostics with various measurements of image degradation. Alternatively, numerical simulations can be used to provide preliminary checks for uniform propagation environments. This section describes a series of measurements that were performed to test the short-term coherence function and beam-wander concepts.

VI.2 Propagation Model

The propagation of a spherical wave can be derived from the relation

$$\frac{\exp\{ikr\}}{4\pi r} = \int\int \frac{i\exp\{ikg(K)|z|\}}{2kg(K)} \exp\{i\mathrm{K}\cdot\rho\}\,\mathrm{dK}/(2\pi)^2, \tag{78}$$

which shows that $i\exp\{ikg(K)|z|\}/(2kg(K))$ is the two-dimensional Fourier transform of the outward-propagating spherical wave in a constant z plane. Forward propagation to any other plane is achieved by applying the propagation factor $\exp\{ikg(K)\Delta z\}$, which simply extends the z component. Any attempt to approximate this relation numerically, however, is futile because of the slow decay of the field. The integral itself is defined only in a special mathematical sense.

The problem can be avoided by using a divergent beam, which retains the phase variation spherical wave but imposes a gaussian intensity profile. For a beam wave,

$$\psi_b(\rho,z) = \frac{1}{1+i\alpha z}\exp\{ikz - \frac{k\alpha}{2}\frac{\rho^2}{1+i\alpha z}\}, \tag{79}$$

where $\alpha = \alpha_r + i\alpha_i$ with

$$\alpha_r = \frac{2}{kW_0^2} \tag{80}$$

$$\alpha_i = \frac{1}{R_0} \tag{81}$$

As discussed previously, the beam size at $z = 0$ is W_0, and R_0 is the curvature of the phase front. For a focused beam, the beam intensity spread reaches a minimum size ω_0

at $z \approx R_0$. The beam size as a function of distance from this minimum is given by the relation

$$W(\bar{z}) = \omega_0 \sqrt{1 + \frac{\lambda^2}{\pi^2 \omega_0^4} \bar{z}^2}. \tag{82}$$

At large distances, the angular extent of the beam is $\lambda/(\pi\omega_0)$. Thus, the beam is well approximated numerically if the spatial wavenumber at the maximum angular deviation is resolved. This leads to the sampling condition

$$\Delta x << \pi\omega_0/2. \tag{83}$$

The number of points needed is determined by the size of the beam at the position where the propagation disturbance is applied.

Following Martin and Flatté [4] we simulate the effects of strong turbulence by multiplying the beam field by a complex random field whose phase autocorrelation function is given by 12 and 13 using the model summarized in Table 1. The location of the phase screen is chosen so that the beam is well tapered over the finite extent of the phase screen. We then propagate the distorted beam wavefield forward by performing a Fourier transform and then multiplying each Fourier component by the propagation factor $\exp\{ikg(K)\Delta z\}$. Strict adherence to the parabolic wave equation requires repetition of this process, but experience has shown that the field statistics well removed from the phase screen are not significantly different if a single phase screen corresponding to the total path-integrated disturbance is used.

In Martin and Flatté's work, multiple phase screens were used, but they simulated only the intensity of the scattered field. To simulate the blurring effects of the turbulence in an image, we have numerically refocused the beam to $\bar{z}$. This is accomplished by back propagating the disturbed beam wavefield through the phase screen location to the point of minimum beam diameter. The same FFT procedure is used to implement the back propagation. In the absence of a phase disturbance, we obtain a small spot as would be observed with a telescope pointed along a focused laser beam. Thus, we use a focused 1.064 μm-beam with a 1-cm waist diverging to approximately 30 cm at the phase screen. The phase screen was placed approximately 2/3 of the distance from the beam waist to the aperture plane.

Figures 5, 6, and 7 show the effects of weak, moderate, and severe turbulence, respectively. The structure constant and the path length within the disturbed medium are listed in the figures. The distances are real units at the location of the beam minimum. Each realization of the focused image can be thought of as an instantaneous field sample as could be obtained, for example, by a video tape recording of the beam focused on a screen. Long-term averages are obtained by incoherently averaging a large number of realizations. Figures 1, 2, and 3 suggest, however, that the beam centroid is

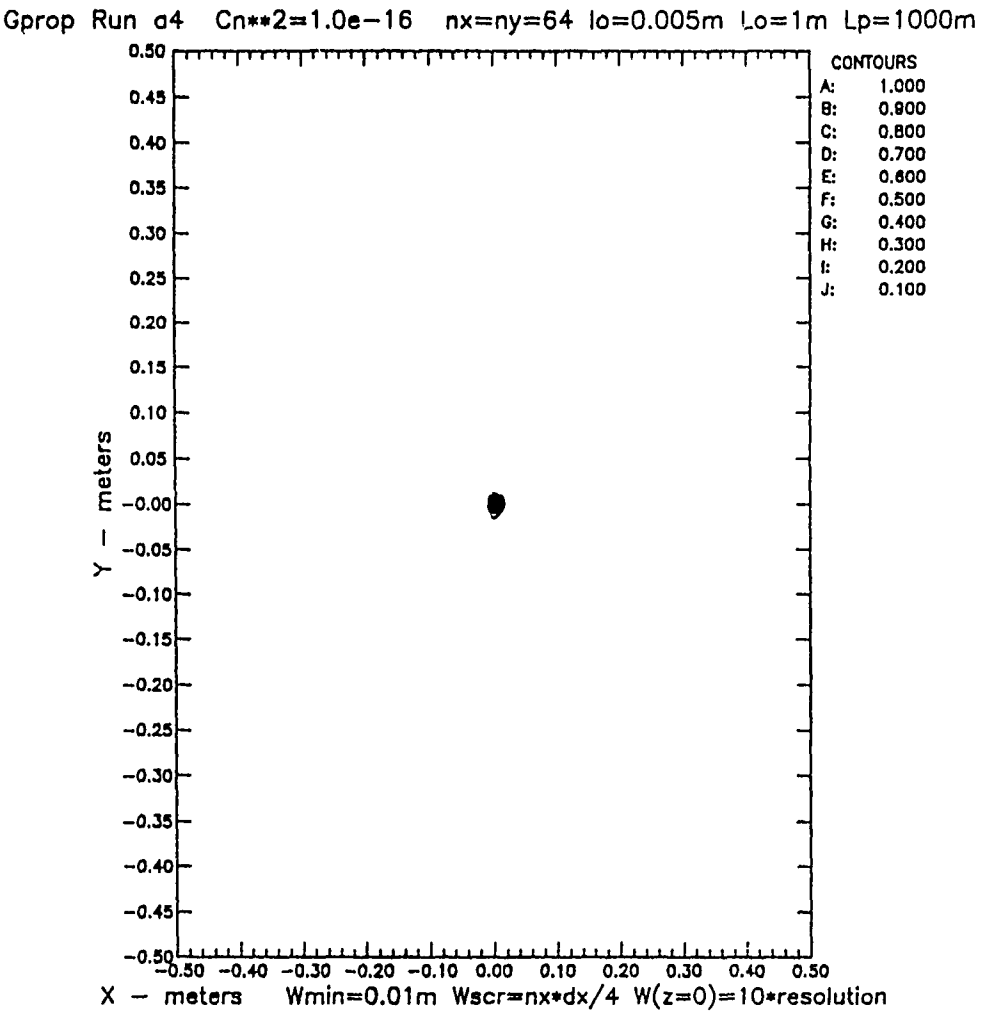

Figure 5. Focused beam simulation for weak turbulence.

near the origin, with very little deviation. We shall see in the next section that this is indeed the case.

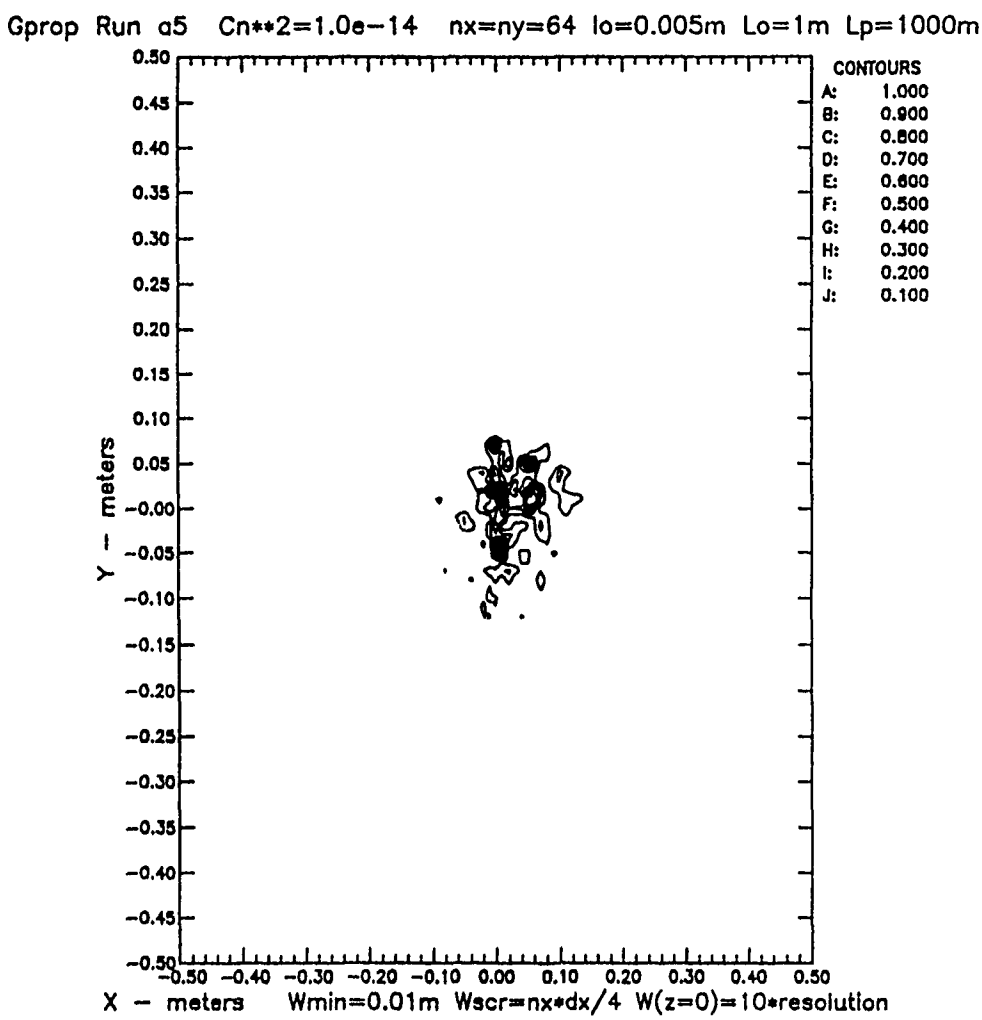

Figure 6. Focused beam simulation for moderate turbulence.

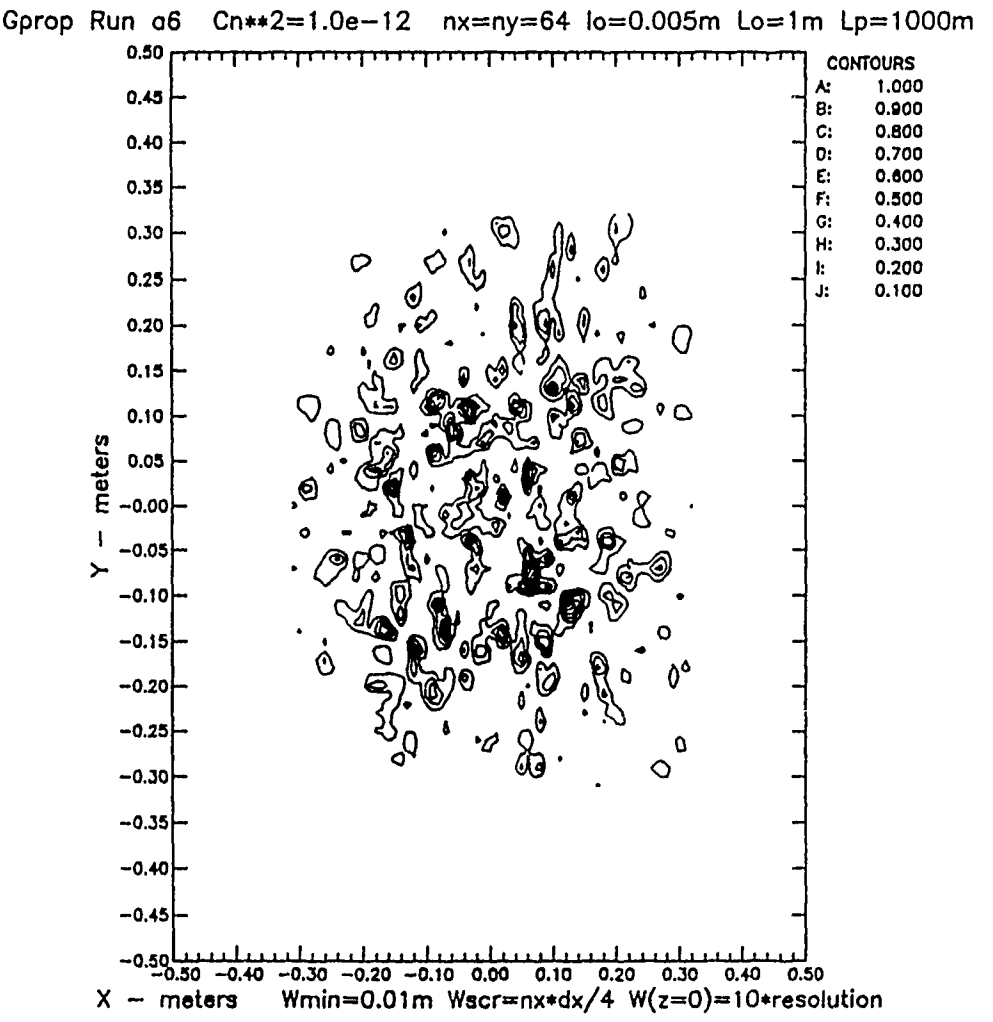

Figure 7. Focused beam simulation for strong turbulence.

VI.3 Summary Statistics

To summarize the average blurring effects or long-time images, we generated a large number of independent realizations for several different turbulence levels and computed standard measures of image degradation. The first moment and second central moment of the image intensity along the reference coordinate directions measure average displacement and image spread, respectively. We also computed the autocorrelation function of each image as a measure of its fine structure. Finally, we computed the autocorrelation function of the average intensity of a large number of independent realizations as a measure of the long-term average spot size.

As a measure of the potential effects of the turbulence, we compute the reciprocal of the e^{-1} decorrelation distance at the aperture plane for the theoretical mutual coherence function. In the IMTURB code, the coherent spot diameter is inversely proportional to the coherence scale. Thus, we have presented the simulation results in terms of the reciprocal coherence scale. To provide a unitless measure, the coherence scale should be normalized to the aperture size; however, only a single aperture size was used for this set of simulations.

Figures 8, 9, 10, and 11 show the average of the measured first and second moments. Because the turbulence is isotropic, we expect and observe no average displacement or difference between the x and y cuts. Although the spread in the displacement increases with increasing perturbation strength, the *wander* is much smaller than the average spread. Thus, if the images were displayed sequentially, no beam wander would be apparent. In short, the homogeneous turbulence model does not contain sufficient low spatial-frequency content to account for the beam wander that is typically observed in experiments.

The most interesting result is summarized in Figure 12, which shows the average short- and long-term structure measures. The long-term beam size starts at twice the focused spot size because of the autocorrelation function measure. As the turbulence develops, however, the long-term beam size increases linearly against the inverse coherence scale, as do the second moments shown in Figures 10 and 11. This confirms the known inverse proportionality between the average focused spot size and the coherence scale at the aperture plane.

The increase in the short-term structure size, however, is not linear with inverse coherence scale. This is possibly due to Fresnel-radius effects, which are intimately part of intensity fluctuations. In any case, we see that the short-term image coherence scale increases at an increasing rate as a function of inverse coherence scale. It is well known that short-term exposures can be refocused to remove the blurring with adaptive phase compensation schemes. We suspect that the short-term coherence scale presented here represents the best that can be achieved with such schemes. For example, in very strong

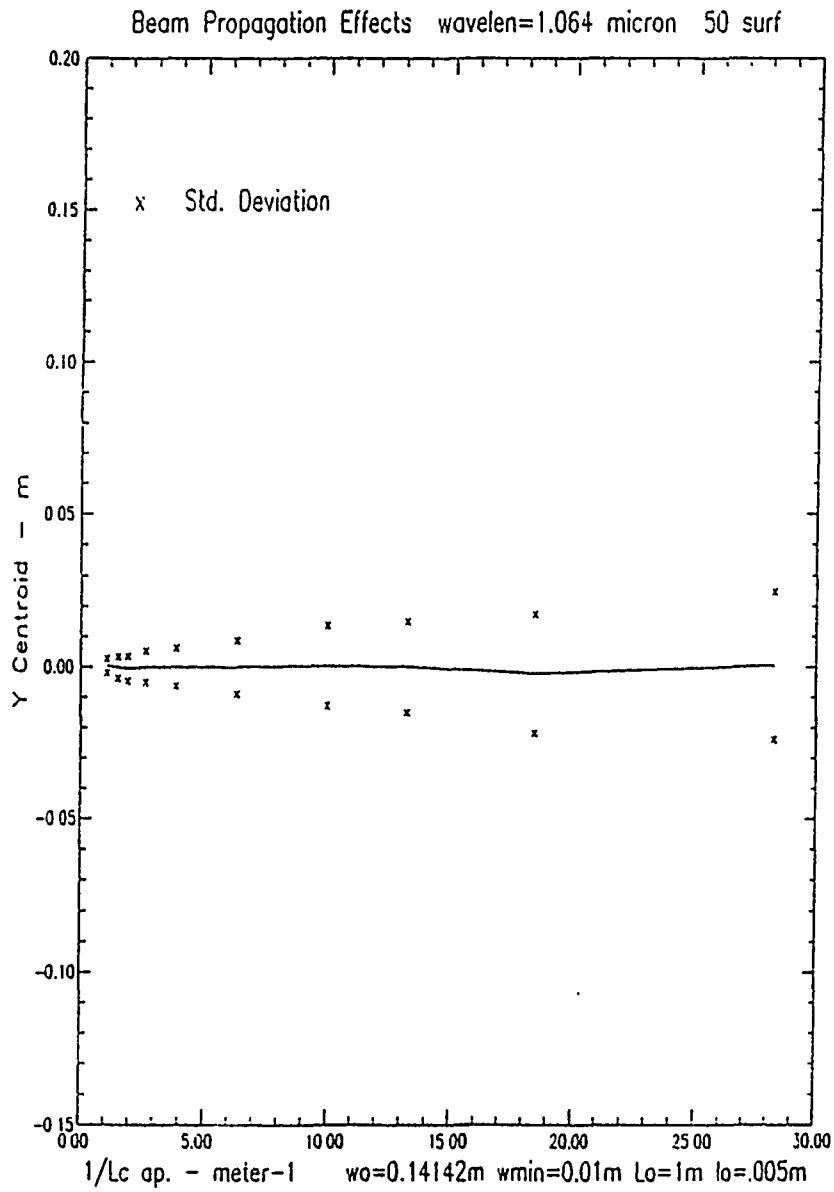

Figure 8. Average beam displacement along x-axis.

turbulence, adaptive focusing can recover only about 50% of the diffraction limited resolution. If this can be confirmed by simulating adaptive phase reconstruction, it will provide an improved quantitative measure of the short-term spot size currently provided by the IMTURB code.

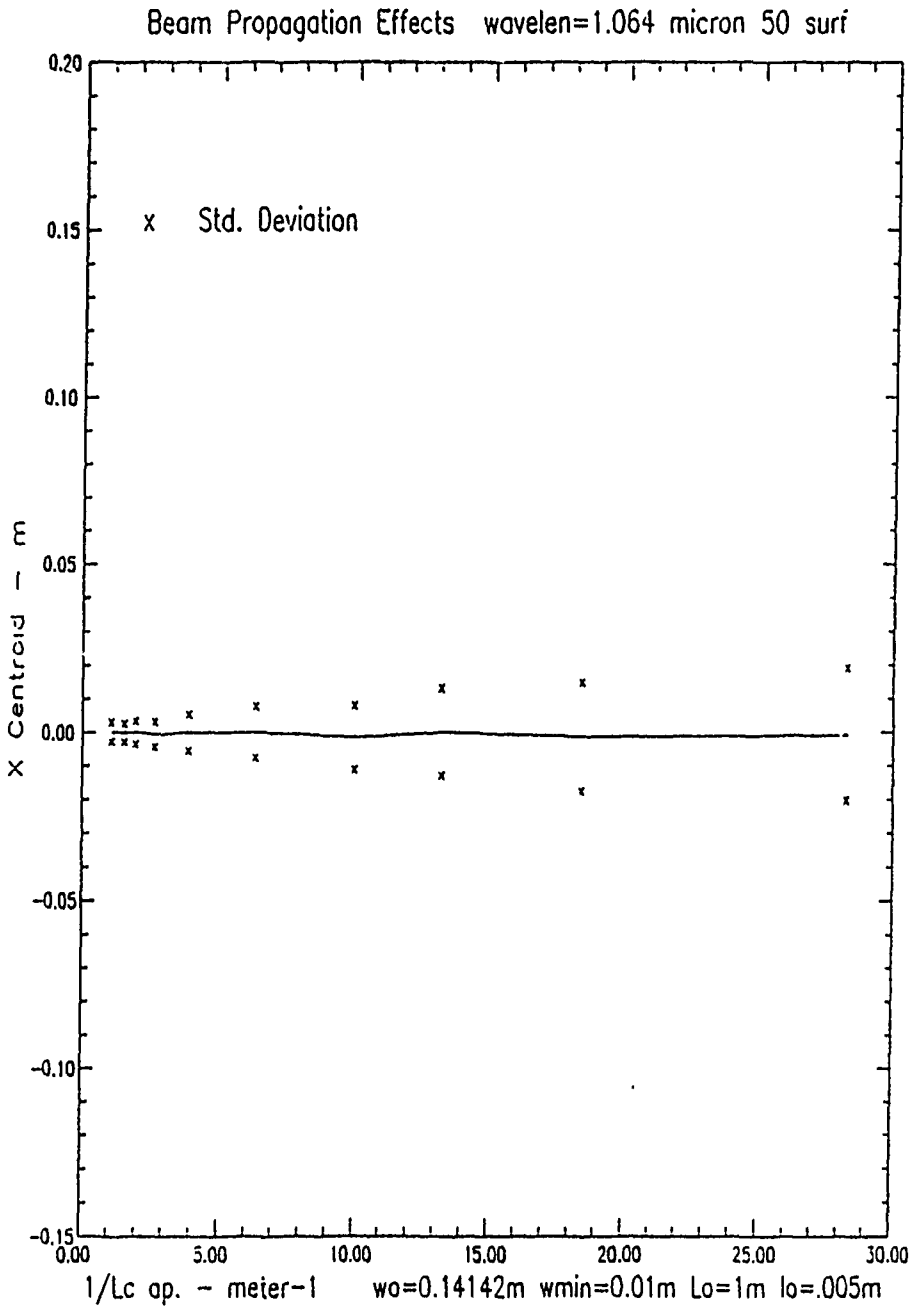

Figure 9. Average beam displacement along y-axis.

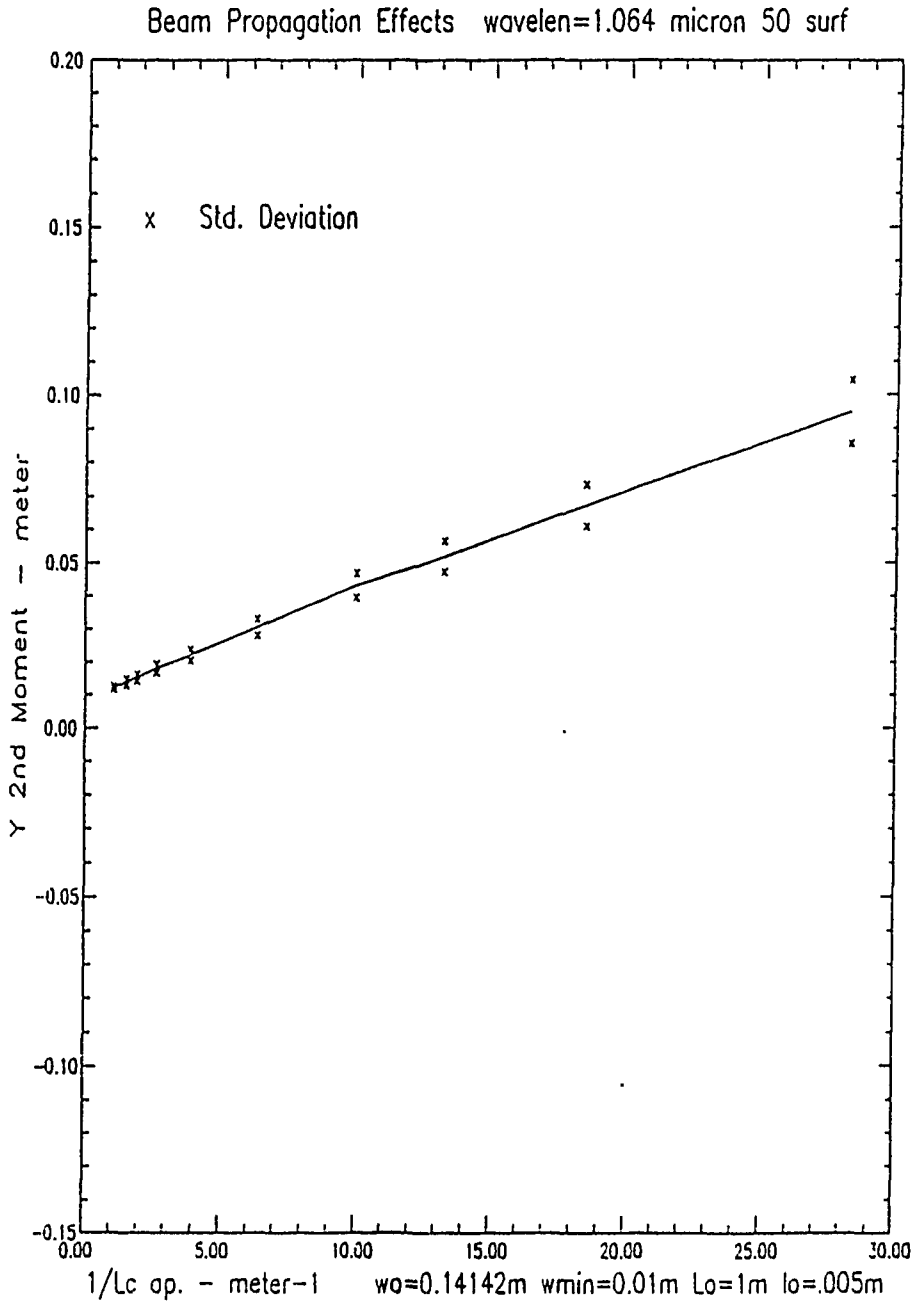

Figure 10. Average beam spread along x-axis.

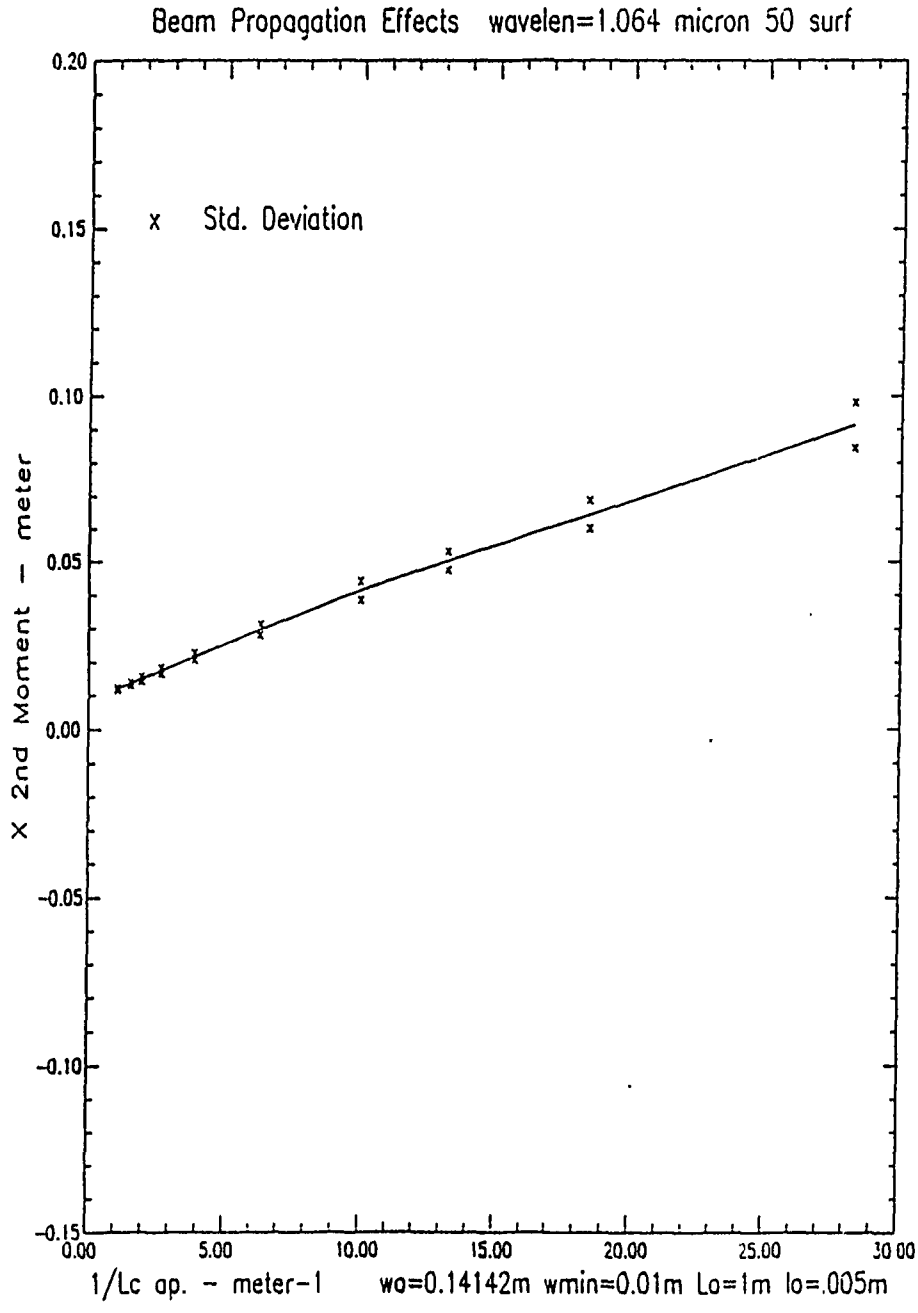

Figure 11. Average beam spread along y-axis.

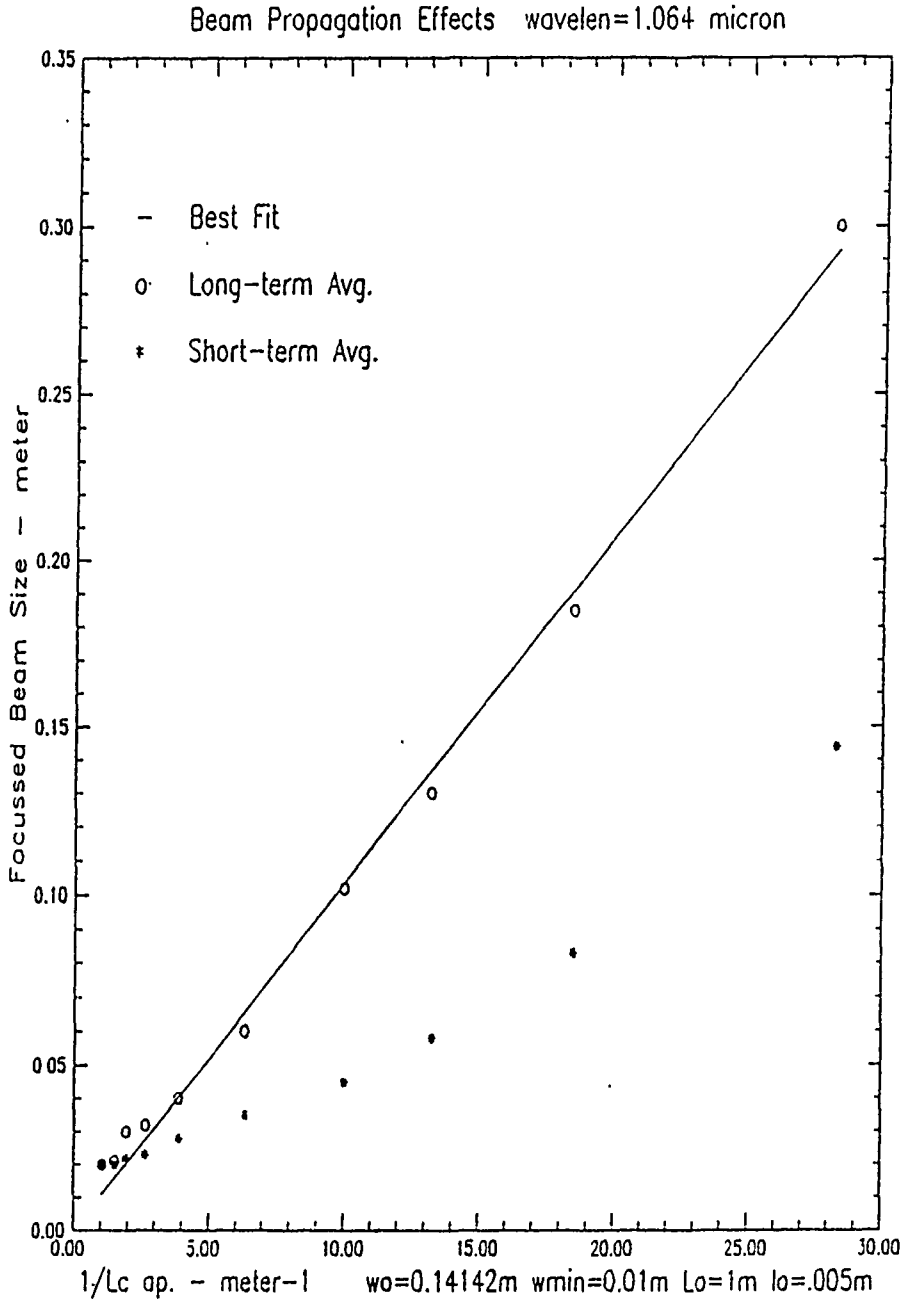

Figure 12. Long- and short-time image correlation measures.

VII Conclusions and Recommendations

A consistently formulated propagation model has been described for systems-oriented predictive codes. The primary model inputs—the structure constant and the outer and inner scale sizes—can be obtained from atmospheric turbulence models. In terms of simple path integrals, the complete mutual coherence function for plane-waves, point sources, and beams can be computed. In fact, the plane and point source limits are special cases of the beam wave result. The model eliminates the restrictions imposed by the Rytov approximation.

Because of the importance of image processing and adaptive compensation of atmospheric turbulence, we also implemented a consistent measure of the short-term coherence scale. As with all previous measures, however, there is no firm theoretical foundation for the result. Thus, we used numerical simulations to study the relation between the long-term and short-term correlation scales. Moreover, in our introductory background material, we showed that any model based on the assumption of locally homogeneous statistics eliminates phase wander that is inherently part of any real propagation environment. Our simulations confirm that slow beam wander is not part of standard homogeneous turbulence models. To the extent that it needs to be included in predictive models, it must be accommodated explicitly.

More importantly, we developed a quantitative measure of the short-term intensity coherence. We don't know how to calculate the measure theoretically, but it could easily be modeled empirically. As noted in Section VI, we believe that the short-term coherence scale as we defined it is a quantitative measure of what can be achieved by adaptive focusing. Future work should test this concept. Beyond that, further improvements to the IMTURB code should be coordinated with field measurements. In a separate memorandum, we have described a simple and cost-effective laser diagnostic system that could achieve this objective.

Appendix

Optical Systems

Ultimately, the wave fields that have been characterized in this report are detected and processed by an optical system. The performance of the optical system for its intended purpose is critically dependent on its detailed configuration, but there are some aspects that are common to all systems. In this appendix a general model that isolates these common features is described.

A-I A Model for Optical/IR Imaging

Consider the general model shown in Figure A1. Any luminous object can be decomposed into a collection of effective point radiators, but for simplicity let $O(\xi)$ represent a collection of noninteracting point radiators that are visible to the optical system. Let $\Delta S_R(\rho, \xi)$ represent the complex wave field in the aperture plane of the receiver from a unit point radiator at ξ. For example, in free space,

$$\Delta S_R^0(\rho, \xi) = \frac{\exp\{ikr\}}{r}, \tag{A1}$$

where

$$r = \sqrt{R^2 + 2\mathbf{R} \cdot (\rho - \xi) + |\rho - \xi|^2}. \tag{A2}$$

It follows from the linearity of Maxwell's equations that the aperture-plane signal from any extended luminous object can be represented by the integral

$$S_R(\rho) = \int_{\text{object}} \Delta S_R(\rho, \xi) O(\xi)\, d\xi. \tag{A3}$$

If the luminosity is broadband, (A3) must be integrated over the temporal frequency spectrum, but the narrowband model is adequate to illustrate the linear systems approach. The complex signal $S_R(\rho)$ over some finite aperture A is accessible to the imaging system for processing. The form of (A3) is the general representation of a spatially varying linear system.

The simplest optical system uses a collection of lenses that effectively apply phase compensation for the propagation paths to ρ from each point in the object space, ξ_0.

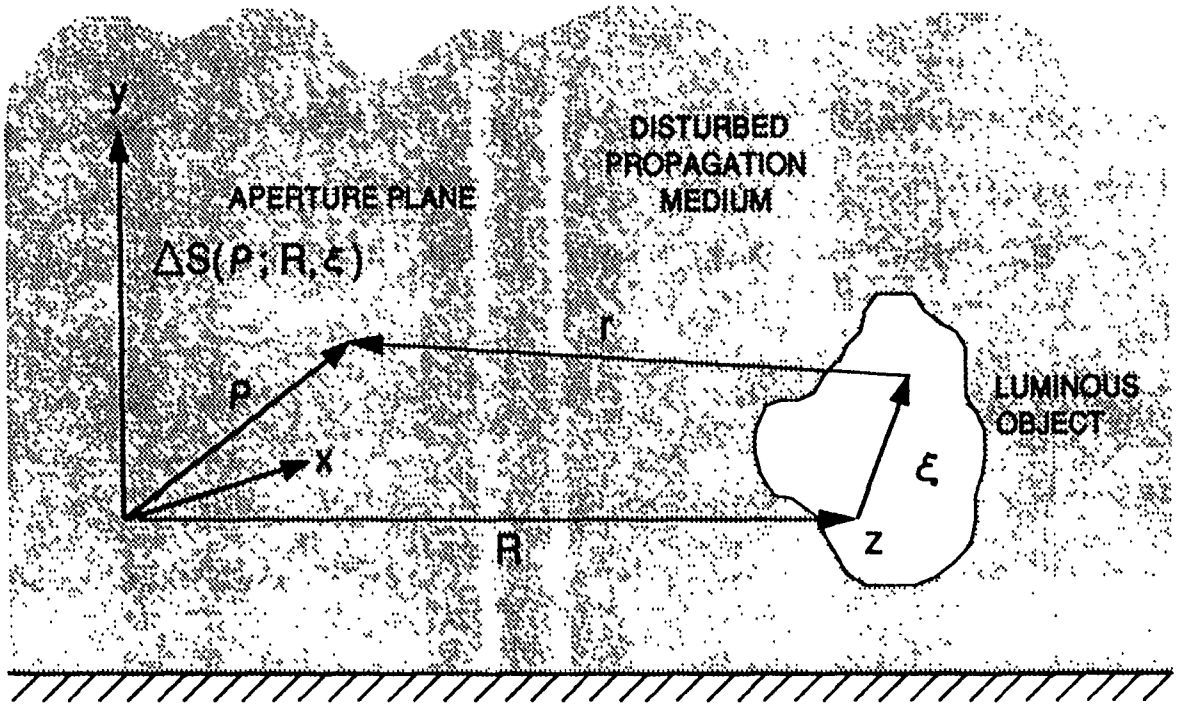

Figure A1. Geometry for general imaging model.

This operation can be represented mathematically as

$$\begin{aligned} V(\xi_0) &= \int_A S_R(\rho) \exp\{i\psi_R(\rho, \xi_0)\}\, d\rho \\ &= \int_A \int_{\text{object}} \Delta S_R(\rho, \xi) O(\xi)\, d\xi \exp\{i\psi_R(\rho, \xi_0)\}\, d\rho. \end{aligned} \tag{A4}$$

The second form is obtained by substitution from (*A*3). Changing the order of integration in (*A*4) gives the linear systems representation

$$V(\xi) = \int_{\text{object}} M(\xi, \xi_0) O(\xi)\, d\xi \tag{A5}$$

where

$$M(\xi, \xi_0) = \int_A \Delta S_R(\rho, \xi) \exp\{i\psi_R(\rho, \xi_0)\}\, d\rho \tag{A6}$$

is the complex point spread function for the imaging system. For an ideal system, $M(\xi, \xi_0) \cong \delta(\xi - \xi_0)$ times an arbitrary phase constant.

Over at least a limited portion of the receiving aperture, the point spread function of a good imaging system will depend only on the difference between the object and target coordinates. Thus, the first step in any imaging process is mathematically equivalent to applying a homogeneous spatial filter to the object illumination. The differences between coherent and incoherent systems manifest themselves in the characteristics of the image intensity, particularly its temporal and spatial coherence properties. In all cases, however, if propagation disturbances are present, the point response function itself acquires a random time-varying component.

A-II Propagation Disturbances in Optical Systems

To identify the random component induced by the propagation disturbances explicitly, let

$$\Delta S_R(\rho, \xi) = H_R(\rho, \xi) \Delta S_R^0(\rho, \xi). \tag{A7}$$

Now consider an object whose luminosity is uncorrelated from point to point and independent of the propagation disturbance. It follows from $(A5)$ that

$$<|V(\xi_0)|^2> = \int_{\text{object}} <|M(\xi, \xi_0)|^2><|O(\xi)|^2>\, d\xi, \tag{A8}$$

where the angle brackets denote ensemble averaging. Similarly, from $(A6)$ it follows that

$$\begin{aligned} <|M(\xi, \xi_0)|^2> \;=\; & \int_A \int_A <H_R(\rho, \xi) H_R^*(\rho', \xi)> \Delta S_R^0(\rho, \xi) \Delta S_R^{0*}(\rho', \xi) \\ & \times \exp\{i[\psi_R(\rho, \xi_0) - \psi_R(\rho', \xi_0)]\}\, d\rho d\rho'. \end{aligned} \tag{A9}$$

Because $R >> \rho$ or ξ, $(A2)$ can be expanded to terms that are quadratic in R^{-1}, whereby

$$\Delta S_R^0(\rho, \xi) \Delta S_R^{0*}(\rho', \xi) \approx \exp\{-ik\Delta\rho \cdot \xi / R\}, \tag{A10}$$

to terms that do not depend on ξ or are quadratic in $\xi/\sqrt{R}$. For an imaging system, there is a similar relation for ψ_R with R replaced by $2f$, where f is the focal length. Also, in Section III.1 we showed that

$$\Gamma(\Delta\rho; \xi, R) = <H_R(\rho, \xi) H_R^*(\rho', \xi)> \Delta S_R^0(\rho, \xi) \Delta S_R^{0*}(\rho', \xi), \tag{A11}$$

so that

$$<H_R(\rho, \xi) H_R^*(\rho', \xi)> = \exp\{-H(\Delta\rho, \xi; R)\}. \tag{A12}$$

Here we have allowed for a weak dependence of $H(\Delta\rho, \xi; R)$ on ξ. If this dependence is neglected, the propagation disturbance is isoplanatic. Finally, we define the function $W(\rho)$ to be unity on A and zero elsewhere and introduce the new variables

$$\eta = k\xi/R \qquad (A13)$$

$$\eta_0 = k\xi_0/(2f). \qquad (A14)$$

With these definitions and approximations, it follows that

$$<M(\eta, \eta_0)> \approx \int F(\Delta\rho) \exp\{-H(\Delta\rho, \eta R/k; R)\} \exp\{-i\Delta\rho \cdot \Delta\eta\}\, d\Delta\rho, \qquad (A15)$$

where

$$F(\Delta\rho) = \int W(\chi + \Delta\rho) W(\chi - \Delta\rho)\, d\chi. \qquad (A16)$$

If there is no propagation disturbance, $H \equiv 1$, and from $(A15)$ we see that the point spread function $M(\Delta\eta)$, which is no longer random, and $F(\Delta\rho)$ form a Fourier transform pair. Analogous to the impulse response-transfer function relation for linear filters, $F(\Delta\rho)$ is called the modulation transfer function (MTF) for the optical system. Note that Goodman [13] uses the terminology optical transfer function. If the disturbance is isoplanatic, we can define an average MTF as

$$<F(\Delta\rho)> = F(\Delta\rho) \exp\{-H(\Delta\rho; R)\}. \qquad (A17)$$

Equation $(A17)$ is the long-exposure MTF for an optical system—see Fried's equations (3.15) and (3.16)[14].

With short exposures it is well known that one obtains a sharper image that is displaced from its center point. It is mainly the slow meandering of the diffracted beam that contributes to the blurring of a point image. To estimate the short exposure MTF, it is clear that one should apply a high-pass spatial filter to $(A7)$ before performing the ensemble average in $(A6)$. Unfortunately, this does not yield mathematically tractable results, and various other schemes have been used. Fante [15, 12], for example, has modified the lower limit of integration in (17) from 0 to $\gamma\Delta\rho/D$, where $\gamma \approx 1$, and D is the size of the largest unresolved eddy, but he remains skeptical of the procedure [16]. Fried [14] removes the least-squares estimate of the linear-phase component; however, the general area of tilt correction merits a more thorough treatment. At the present time, however, there is no satisfactory analytical approximation for the short-term MTF.

References

[1] David L. Fried. Theoretical study of non-standard imaging concepts. Final Report RADC-TR-76-51, Optical Science Consultants, 1976.

[2] Walter B. Miller and Jennifer C. Ricklin. IMTURB: A module for imaging through optical turbulence. Preliminary document, U.S. Army Atmospheric Sciences Laboratory, 1989.

[3] C. L. Rino and Angela Regalia. An improved propagation model for optical and ir imaging. Final report, Vista Research, Inc., 1989. U. S. Army Atmospheric Sciences Laboratory Contract DAAL03-86-D-0001.

[4] J. M. Martin and Stanley M. Flatté. Simulation of point-source scintillation through three-dimensional random media. *J. Opt. Soc. Am. A*, 7(5):838–847, 1990.

[5] I. P. Shkarofsky. Generalized turbulence space-correlation and wave-number spectrum-function pairs. *Canad. J. Phys.*, 46(19):2133–2153, 1968.

[6] C. L. Rino and E. J. Fremouw. The angle dependence of singly scattered wavefields. *J. Atmos. Terr. Phys*, 39:859–868, 1977.

[7] A. Ishimaru. *Wave Propagation and Scattering in Random Media–Vol 2, Multiple Scattering, Turbulence Rough Surfaces, and Remote Sensing.* New York: Academic Press, 1978.

[8] C. L. Rino. A power-law phase-screen model for ionospheric scintillation: 2. Strong scatter. *Radio Science*, 14(6):1147–1155, 1979.

[9] C. L. Rino and J. Owen. Numerical simulations of intensity scintillation using the power law phase screen model. *Radio Science*, 19(3):891–908, 1984.

[10] A. M. Whitman and M. J. Beran. Two-scale solution for atmospheric scintillation. *J. Opt. Soc. Am. A*, 2(12):2133–2143, 1985.

[11] J. M. Martin and Stanley M. Flatté. Intensity images and statistics from numerical simulation of wave propagation in 3-D random media. *Applied Optics*, 27(11):2111–2126, 1988.

[12] Ronald L. Fante. Electromagnetic beam propagation in turbulent media. *Proc. IEEE*, 63(12):1669–1692, 1975.

[13] Joseph W. Goodman. *Statistical Optics.* New York: John Wiley & Sons, 1985.

[14] David L. Fried. Optical resolution through a randomly inhomogeneous medium for very long and very short exposures. *J. Opt. Soc. Am.*, 56(10):1372–1379, 1965.

[15] Ronald L. Fante and Richard L. Taylor. Short-term spot size and beam wander in a turbulent medium. Research Paper AFCRL-TR-74-0595, Air Force Cambridge Research Laboratories, 1974.

[16] Ronald L. Fante. Electromagnetic beam propagation in turbulent media: An update. *Proc. IEEE*, 68(11):1424–1443, 1980.